QUANTITATIVE METHODS FOR ANALYSIS OF TSPO AVAILABILITY IN PROGRESSIVE MULTIPLE SCLEROSIS, USING BRAIN PET IMAGING WITH RADIOLIGAND ^{11}C-PBR28

MOHAMMAD KAFAMI KHORASANI

Master's Thesis

Turku Brain and Mind Center
Faculty of Medicine
University of Turku
May 2021

M.Sc. Human Neuroscience

Supervisors Prof. Laura Airas, MD, PhD
Markus Matilainen, PhD
Technical Advisor Jouni Tuisku, PhD
Reviewers Prof. Laura Airas, MD, PhD
Vesa Oikonen, MSc

University of Turku
Faculty of Medicine
MDP in Human Neuroscience
Mohammad Kafami Khorasani

QUANTITATIVE METHODS FOR ANALYSIS OF TSPO AVAILABILITY IN PROGRESSIVE MULTIPLE SCLEROSIS, USING BRAIN PET IMAGING WITH RADIOLIGAND ^{11}C-PBR28

Master's Thesis
13.12.2021

ABSTRACT

Background – The translocator protein 18kDA (TSPO) is closely related to diffuse inflammatory demyelinating injury and hence represents an ideal target for brain imaging in progressive-MS pathology in vivo. However, quantification of the TSPO is associated with number of challenges corresponding to its genetic polymorphism and localization in the CNS and surroundings. Subsequent inaccuracy in TSPO quantification with plasma concentration or anatomical brain reference region proposes for implementation of alternative quantification approaches that are hypothesized to compensate the shortcomings.

Objectives – This study has tried to perform a comparative evaluation of novel quantification approaches for analyzing neuroinflammation using ^{11}C-PBR28 tracer in MR-PET brain imaging of the patients with SPMS versus healthy control participants.

Methods – Nine secondary progressive MS and 11 healthy controls have been examined in 3Tesla MR and (^{11}C-PBR28) PET brain imaging in Turku PET Centre (TPC). Brain segmentation and image preprocessing were fulfilled using Freesurfer v.5.3 and SPM12 toolset in MATLAB. Lesion and ROIs delineation was performed via in house software. Tracer binding activity was measured, and volume of distribution was quantified via 2TCM compartmental model. Four brain reference regions were considered for normalization of the values, consisted of three anatomical reference regions in addition to one supervised clustering pseudo-references modified version of the algorithm developed in the Harvard university for similar aim.

Results – The results of this study obtained via examination of several kinetic models, data and partial volume correction steps aimed at narrowing down the selected approaches and accounting the apparently most robust method for the higher-level analysis and the statistical examination. However, through neither of the steps any result represented a significant support for the H_1 hypothesis in this study.

The low signal to noise ratio of the PET imaging data with the utilized radioligand and the diffusivity of the TSPO in the MS brain, along with the complexity of quantification caused by the polymorphism genotype and the affinity binding of the radiotracer in MS brains and blood plasma are the greatest obstacles challenging the analysis of the PET-MR imaging data in the pathological studies of the MS in vivo.

Keywords: ^{11}C-PBR28, Kinetic modeling, Microglia, Multiple Sclerosis, PET-MR Imaging, TSPO

To my wife who has always supported me with open heart,
and to my little son whose smile is the lodestar along the way.

ABBREVIATIONS

18kDa	18 kilo-Dalton translocator protein
2TCM	2 Tissue, 3 Compartment Model
AAL	Automated Anatomical Labeling
AD	Alzheimer Disease
BBB	Blood Brain Barrier
BP	Binding Potential
BP_{ND}	Non-displaceable Binding Potential
Bq	Becquerel
CIS	Clinically Isolated Syndrome
CNS	Central Nervous System
CSF	Cerebrospinal Fluid
DIT	Dissemination in Time
DIS	Disseminations in Space
DMT	Disease Modifying Therapy
DTI	Diffusion Tensor Imaging
DV	Distribution Volume
DVR	Distribution Volume Ratio
EDSS	Expanded Disability Status Scale
FA	Fractional Anisotropy
FLAIR	Fluid Attenuated Inversion Recovery
GM	Gray Matter
HAB	High Affinity Binder
HC	Healthy Controls
HD	Huntington's Disease
HRRT	High Resolution Research Tomography
K_d	Dissociation Constant
LAB	Low affinity Binder
LST	Lesion Segmentation Tool
MAB	Mixed Affinity Binder
MRI	Magnetic Resonance Imaging
MS	Multiple Sclerosis

NAGM	Normal Appearing Gray Matter
NAWM	Normal Appearing White Matter
PBR	Peripheral Benzodiazepine Receptor
PD	Parkinson's Disease
PET	Positron Emission Tomography
PPMS	Primary Progressive MS
PVE	Partial Volume Effect
PVC	Partial Volume Correction
RF	Radiofrequency
ROI	Region of Interest
RRMS	Relapsing Remitting Multiple Sclerosis
SD	Standard Deviation
SNR	Signal to Noise Ratio
SPM	Statistical Parametric Mapping
SPMS	Secondary Progressive Multiple Sclerosis
SUV	Standardized Uptake Value
SVCA	Supervised Cluster Algorithm
TAC	Time Activity Curve
TSPO	Translocator Protein
V_T	distribution volume
WM	White Matter
µg	Microgram

Table of Contents

1. INTRODUCTION

Multiple sclerosis (MS) is an inflammatory neurodegeneration disease of the central nervous system (CNS) accompanied by diffuse and focal lesions and axonal demyelination induced by immunogenic processes within the brain and spinal cord. The Secondary Progressive Multiple Sclerosis (SPMS) as the most common progressive form of the disease is characterized by worsening neurological and physical disability over the time. Moreover, it is associated with chronic plaques, diffuse inflammatory process with widespread activation of microglia and axonal degradation, within the normal appearing white (NAWM) and gray matter (NAGM). Unfortunately, there is no curative remedy for multiple sclerosis, and so far, the therapeutic and medical approaches are restricted to disease modifying therapy (DMT) that would only help reducing the intensity of the occurring symptoms and suppressing the inflammatory activities (Costello et al., 2014). During the past decades, despite considerable improvement with developing of such treatments for RRMS, there is still only few therapeutic approaches for SPMS (Inojosa et al., 2021). Furthermore, the belated diagnosis of SPMS and transition from RRMS have been a principal obstacle for delivering a prompt and effective treatment to the patients. However, defining methods and solutions to facilitate the early diagnosis could open a window of opportunities to attain curative therapy of MS (Inojosa et al., 2021).

Neuroinflammation and activated glial cells, predominantly microglia are found to be the main driving forces of the neurodegeneration, demyelination, and axonal death in MS (Chen & Guilarte, 2008; Compston & Coles, 2008). The 18 Kilo-Dalton translocator protein (18kDa / TSPO) first described as Peripheral benzodiazepine Receptor (PBR) is highly upregulated inside the glial cells, and in smaller extent in reactive astrocytes, as a consistent result of the microglia activation (Veronese et al., 2018). Therefore, it is considered to be an ideal target for positron emission tomography (PET) imaging of neuroinflammation in vivo, as several radio-ligands have been developed with appropriate binding assay to quantify this particular neuroinflammatory disease biomarker.

Along with the clinical examinations and laboratory results, neuroimaging plays a key role in the modern diagnosis and in monitoring of the disease. Despite the outstanding role of MR imaging in the diagnosis and monitoring of MS, this imaging modality lacks sensitivity in terms of dissecting various pathological features in MS brain. In this regard, recent

studies have demonstrated the usability of positron emission tomography to complement MRI-based studies, as PET allows detailed molecular and neuroreceptor imaging in brain in vivo (Sahab et al., 2007; Ziemssen et al., 2019).

For the past 25 years, the TSPO-binding tracer PK11195, labeled with [^{11}C] has been widely used in PET imaging of the neuroinflammation (Sucksdorff et al., 2020). However, the quantification of ^{11}C-PK11195 data poses a number of challenges stemming from either the ligand's affinity to some binding sites in the blood such as platelets and blood proteins (Yaqub et al., 2012) , or/and the extensive distribution of TSPO in the normal brain and blood brain barrier (BBB) (Anderson et al., 2007; Turkheimer et al., 2007), an indication of abundant non-specific binding. These hindrances have motivated the development of novel TSPO ligands referred to as the second-generation ligands. Such practices strive for improving the shortcomings in imaging with ^{11}C-PK11195, for instance signal-to-noise ratio and enhanced quantification outcome in PET data (Chauveau et al., 2008). Thus far, the ideal image quality has not been delivered, which may relate to a number of obstacles such as over intensified TSPO binding on the BBB, restricted instrumentation, and unavailability of tissue reference region, and last but not least, nucleotide polymorphism in the TSPO gene that variates the binding affinity in different participants (Turkheimer et al., 2015).

Tackling such difficulties barricading adequate analysis and quantification requires the implementation of methods that allow identifying the TSPO fraction which specifically represents the inflammatory response due to MS, distinct form the widespread nonspecific binding sites within the CNS and its surroundings (Delforge et al., 1996) Applying such methods, imposes introducing a suitable reference area with similar perfusion characteristics to ones of the target tissue but lacking the ligand's target biomarker. Nonetheless, the heterogeneous distribution of TSPO alongside the unknown localization of microglial activation avoids selecting an anatomical reference region *a-priori* (Turkheimer et al., 2015; Yaqub et al., 2012), and therefore, a pseudo reference region obtained via classification algorithms on voxel clusters in the brain is hypothesized to be a suitable alternative.

Considering the challenges in the conventional methods for quantification of the activity concentration of the radioligand in MS brains, this study has investigated the different mathematical models and quantification approaches aiming to suggest a robust method for

obtaining the most reliable results for this purpose. Several quantification methods including the modeling of different TSPO binding values normalized on bases of both anatomical and supervise clustering pseudo reference region have been selected and implemented for the analysis of the data acquired from SPMS patients compared to that of a group of healthy controls. Accordingly, the results obtained via selected methods have been evaluated and compared to each other, aimed at finding a favorably efficient approach to be suggested to the future progressive MS studies in vivo.

2. REVIEW OF THE LITERATURE

2.1 Multiple Sclerosis

Multiple sclerosis is a chronic autoimmune-mediated disease, characterized by focal and diffuse lesions in the Central Nervous System, resulting from demyelination and neurodegeneration in the white matter (WM) and grey matter (GM) (Filippi et al., 2012; Ziemssen et al., 2019) Neurodegeneration, axonal demyelination, and their corresponding clinical impairment in advance stages of MS are followed by series of life threatening physical and cognitive disability that permanently affects the patients' lives, if not leading to death (Ghasemi et al., 2016). According to World Health Organization (WHO), in 2016 the global prevalence of MS was estimated to 2.3 million, with rate of 35 cases per 100,000 world-wide. The estimated number indicates that the age-standardized prevalence rate of the disease has raised 10.4% since 1990 (Bezzini & Battaglia, 2017; Wallin et al., 2019). Being the most common cause of neuro-traumatic neurological disability among young adults, MS usually occurs between 20 to 40 years of age. However, the disease can affect humans in other age ranges as well. Hence the disease not only jeopardizes the individuals' lives, but also it provokes social and economic burden in the human society (Compston & Coles, 2008b; Lebrun-Frenay et al., 2017).

2.2 Disease course and subtypes

The natural history of MS varies in different patients regarding the span and the severity of the disease (Figure 1). The initial stage in majority of the patients starts with a bout of neurological symptoms suggestive of MS, when the pathological entity is called clinically isolated syndrome (CIS). Relapsing Remitting MS is the most common type of the disease encompassing almost 85-90 percent of the early patients (Compston & Coles, 2008). At this stage, acute symptoms can be fully or partially recovered after the onset, and symptoms may go away over a few days. Nonetheless, a very rare phenotype of the disease, named Primary Progressive Multiple Sclerosis can appear at disease onset in about 10 percent of the cases (Gross & Watson, 2017).

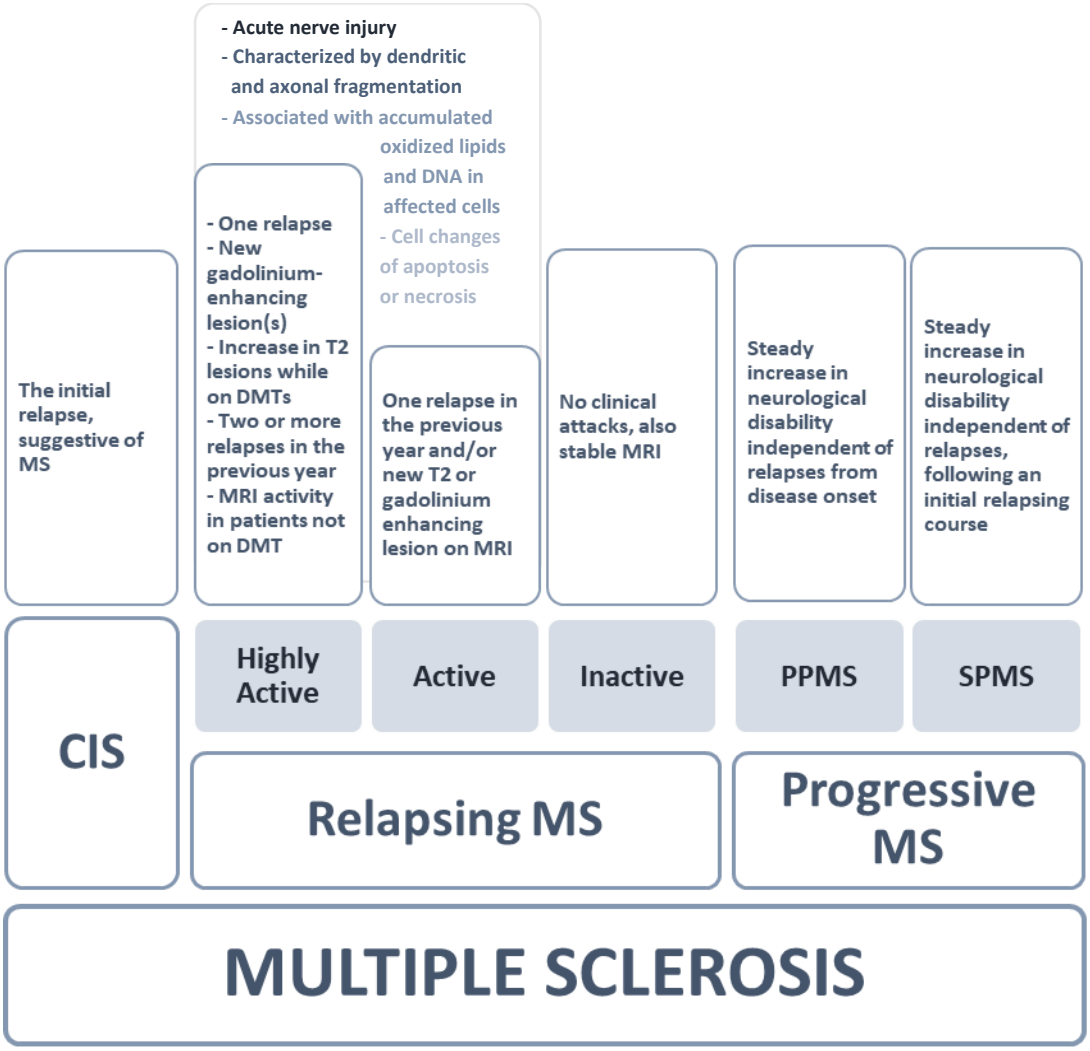

Figure 1. *An overview of the Multiple Sclerosis, different phenotypes, and their key aspects*

A majority of the patients with RRMS, gradually develop worsening disability leading towards the secondary progressive MS after 15 to 35 years from the onset (Compston & Coles, 2008; Kantarci & Weinshenker, 2005). Topography of demyelination and neurodegeneration in SPMS demonstrates a diverse range of vulnerability in different CNS regions. However, the diffuse atrophy, widespread neuroinflammation, microglia activation and axonal damage can appear in the entire central nervous system, including the normal appearing white and gray matter (Chen & Guilarte, 2008; Weinshenker, 1995). A broad number of studies reveal that the major physical impairments of the disease generally appear in vision, muscle control, balance, and autonomic systems due to its effects on the motor-sensory cortices, optic nerve, brain, and spinal cord. However, in

addition to the disease-specific aspects, some patients may experience a group of other symptoms such as Lhermitte's [1], and the Uhthoff [2] phenomena (Compston & Coles, 2008).

2.3 Risk factors and prevalence of MS

It is widely believed that the interaction of multiple genetic and environmental factors are the driving forces of the MS, among which age, sex, vitamin D serum level, experiencing infectious diseases, genetic susceptibility and environmental exposure are the most considerable parameters (Compston & Coles, 2008; Kamel, 2019). Viral infections such as Epstein-barr are also considerably associated with onset of MS. A direct viral injury to the nervous system tissue can result in an autoimmune damage to the myelin by immunogenic exposure of the myelin antigens. On the other hand, molecular emulation between virus antigens and myelin constituents can expose the myelin molecules to the immune response, ending up destroying the myelin sheath (Ascherio & Munger, 2010; Love, 2006).

Statistics indicate that women are twice as men in risk of developing Multiple Sclerosis. There is a familial recurrence rate of 20% with Multiple Sclerosis, with the reduction risk ratio of 3:1 percent, as the relation changes from the fist-degree to second and third-degree relatives. Epidemiology and social-health studies suggest strong evidence for the environmental factors involved in MS. The disease global distribution varies geographically, as increasing with latitudinal distance from the equator. The highest rate with over 100/100 000 has been declared in Scotland and parts of Scandinavia and Canada (Love, 2006). Particularly in Finland, where this study is being performed, the popularity has been estimated to 130/100 000 with annual incidence rate of 7/100 000 until 2014 (Compston & Coles, 2008). Moreover, migration from a high-prevalence to a lower-prevalence area reduces the risk of developing MS in individuals and vice versa (Love, 2006).

[1] Lhermitte's sign appears as electrical signals that radiate downwards in the spine, towards the legs, trunk, and over the limbs at time of wrong neck movement or flexion.

[2] Uhthoff phenomenon is considered as the worsened symptoms following the body temperature elevation, e.g., a hot bath or exercising

2.4 Diagnosis of Multiple Sclerosis

Diagnosis of MS in early stages, particularly in relapsing remitting form, is based on clinical examinations, imaging of CNS and assessment of laboratory parameters such as cerebrospinal fluid (CSF), with regards to a set of principles called McDonald criteria involving the evidence of the disease's dissemination in time (DIT) and space (DIS) (Barkhof et al., 1997; Rissanen, 2015). In subjects of SPMS subtype, even though the diagnostic techniques remain quite similar, the gradual and smooth advancement of the disease alters the assignment of the diagnosis process to any certain classification, as it is for RRMS. Transition from RRMS to SPMS is thought to be a key determinant of long-term disease prognosis (Scalfari et al., 2014). However, imaging criteria and biomarkers are not available for distinguishing RRMS from SPMS. Secondary Progressive MS is diagnosed retrospectively and given that the SPMS is the following advancement of the RRMS, confirmation of this stage is associated with series of examinations to assess (using the expanded disability status scale, EDSS) if the transformation of the disease shows a sign of permanent worsening of disability (Rissanen, 2015).

EDSS is the most popular rating system used for valuation of different stages of disability in the disease, ranging from 0 to 10. Score 0 represents no disability in the subject, whereas 10 implies death due to MS (Rissanen, 2015). Different EDSS scores and their implication are presented in Table 1.

Table 1. *EDSS, summary of the disability scores indication*

Reprinted from (Rissanen, 2015)

EDSS Score	Disability stage
0.0	Normal neurological exam
1.0	No disability, minimal signs in one FS
1.5	No disability, minimal signs in more than one FS
2.0	Minimal disability in one FS
2.5	Minimal disability in two FS
3.0	Moderate disability in one FS though fully ambulatory; or mild disability in three or four FS though fully ambulatory
3.5	Fully ambulatory but with moderate disability in one FS and mild disability in one or two FS and others 0 or 1; or fully ambulatory with two FS grade; or fully ambulatory with five FS grade 2
4.0	Ambulatory without aid or rest for ≥500 meters; up and about some 12 hours a day despite relatively severe disability consisting of one FS grade 4 or combinations of lesser grades exceeding limits of previous steps
4.5	Ambulatory without aid or rest for ≥300 meters; up and about much of the day, characterized by relatively severe disability usually consisting of one FS grade 4 and combination of lesser grades exceeding limits of previous steps
5.0	Ambulatory without aid or rest for ≥200 meters
5.5	Ambulatory without aid or rest for ≥100 meters
6.0	Unilateral assistance (cane or crutch) required to walk at least 100 meters with or without resting (see chapter 8, Ambulation)
6.5	Constant bilateral assistance (canes or crutches) required to walk at least 20 meters without resting (see chapter 8, Ambulation)
7.0	Unable to walk 5 meters even with aid, essentially restricted to wheelchair; wheels self and transfers alone; up and about in wheelchair some 12 hours a day
7.5	Unable to take more than a few steps; restricted to wheelchair; may need some help in transferring and in wheeling self
8.0	Essentially restricted to bed or chair or perambulated in wheelchair, but out of bed most of day; retains many self-care functions; generally, has effective use of arms
8.5	Essentially restricted to bed much of the day; has some effective use of arm(s); retains some self-care functions
9.0	Helpless bed patient; can communicate and eat
9.5	Totally helpless bed patient; unable to communicate effectively or eat/swallow
10.0	Death due to MS

2.5 MS Pathogenesis

Multiple Sclerosis involves neuro-inflammation mediated by T-cells based on the peripheral lymphatic system, migrating through the cerebrospinal fluid, and penetrate the BBB into CNS. The infiltrating T-cells that mediate the inflammation, initiate the tissue injury in the brain and cause axonal demyelination, progressive neurodegeneration, and neuronal death. Neuroinflammation in brief, is referred to as an overactive inflammatory response in the CNS, drawn by a series of mediators resulting from the resident microglia and astrocytes, peripherally derived immune cells, and endothelial cells within the central nervous system (DiSabato et al., 2016). Subsequent effects of neuroinflammation lead to further physiological and immunological defects depending on the neurological pathologies involved. As the disease evolves from the early phase (RRMS) to the Secondary Progressive MS, the inflammatory response itself subsides gradually, whereas oxidative injury and cellular damages become intensified due to patients' aging, disease advancement and the lesion burden (Haider et al., 2016).

Furthermore, innate immune system in the CNS may play a key role in demyelination and axonal degradation in the brain and the spinal cord, mediated by microglia (Haider et al., 2016; Lassmann et al., 2007). Microglia are the central nervous system's macrophages with a major role in its innate immune capacity, present in both gray and white matter of the brain and spinal cord, comprising 10% of the CNS population. These glial cells are the focal point in any neuroinflammation argument, due to their active role in neuroinflammation course (Ginhoux et al., 2013). Microglia propagate the inflammatory signals, initiated in the periphery, as a pivotal response in coordinated communication between the immune system and the brain (e.g., in case of infection, microglia become activated and act as inflammatory mediators). The increased expression of cytokines and activation of microglia in essence, are intended to benefit the host organisms by protecting against the infection and diseases. Contrarily, the amplified or long-term and chronic microglia activation can result in disadvantageous pathological changes and neurological complications (DiSabato et al., 2016).

An important outcome of the activated microglia is the upregulation of the 18 Kilo Dalton translocator protein (TSPO), expressed throughout the entire body and brain, and especially in the glial cells of the brain parenchyma and in smaller extent in reactive astrocytes (Veronese et al., 2018). The translocator protein 18kDa, previously referred to

as Peripheral Benzodiazepine Receptor (PBR), is a ubiquitous cholesterol binding protein highly contained in glandular and secretory organs and with intermediate levels in microglial tissues (*Figure 2*) (Batarseh & Papadopoulos, 2010). TSPO is found to be localized on the outer mitochondrial membrane within the glial cells, involving in various cellular functions such as mitochondrial respiration, cholesterol transportation, cell proliferation and oxidative stress (Batarseh & Papadopoulos, 2010). The activation of microglia caused by active brain diseases is associated with de novo expression of TSPO, increasingly expressed in many cerebral pathological states, like Huntington's disease (HD), MS and brain ischemia (Gerhard et al., 2006; Ouchi et al., 2005). Also, in vivo studies suggest increased TSPO binding in Parkinson's disease (PD) and Alzheimer's disease (AD) alongside microglial activation (Tomasi et al., 2008).

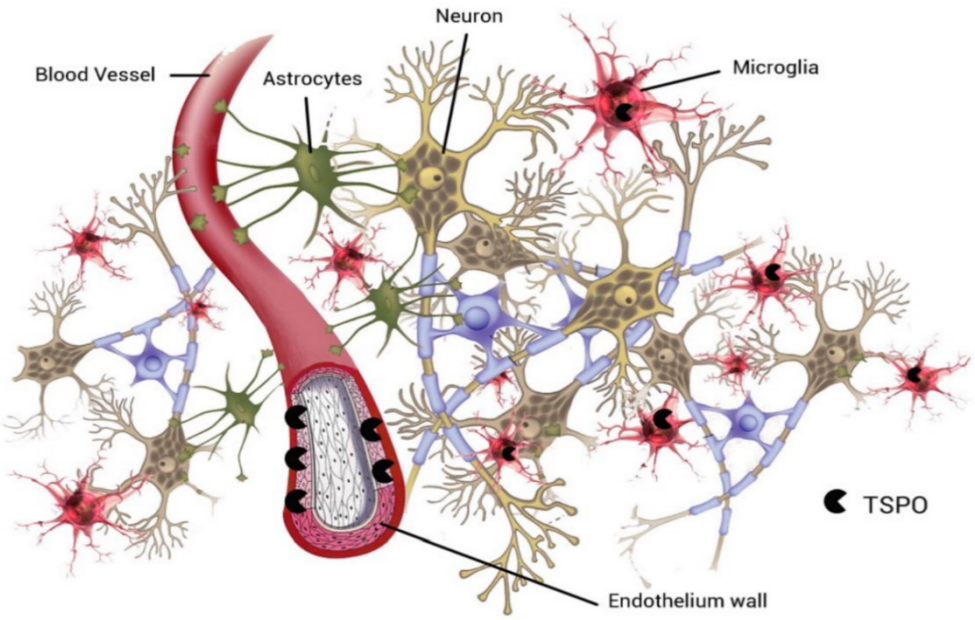

Figure 2. *The presence of abundant TSPO on the endothelium besides activated microglia and macrophages in brain tissue.*

Cropped and reprinted from (Rizzo et al., 2014)

2.5.1 RRMS and SPMS, *distinct characteristics and mechanism*

Early neuroinflammatory events as mentioned above, with direct or indirect impacts on the axonal loss and formation of the lesions, mostly occur in the primary phase of the disease and remain principal causes of the progression in the further stages. However, for better

identifying the behavior of the disease in each stage, illustration of a group of distinct characteristics that vary in different disease phenotypes would be essential. MS lesions, regarding the presence of macrophages and activated

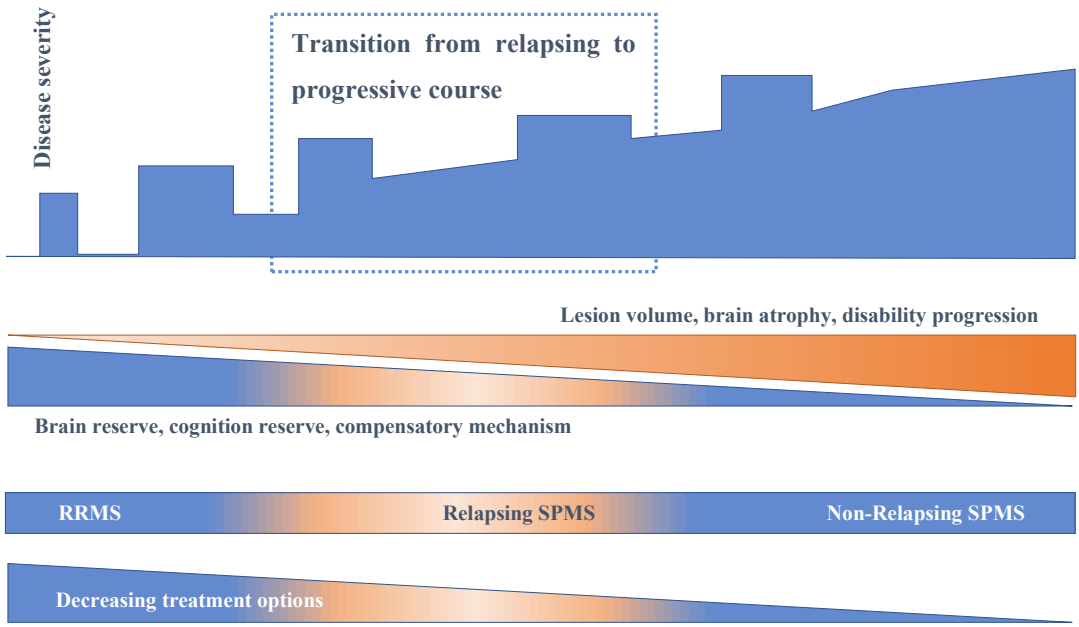

Figure 3. *. Illustration of the transition phase on the natural history of MS, From RRMS to SPMS, the brain reserve, cognitive reserve and other compensatory mechanisms may cover early clinical manifestations of the progressive disease. As these mechanisms are exhausted, patients are more easily aware of newer and progressive symptoms. Similarly, approved treatment options decrease as the disease progresses*

Reprinted from (Inojosa et al., 2021)

Microglia can be categorized into two main groups of 'acute' and 'chronic' lesions, of which the former is closely infiltrated by macrophages consisting of demyelinating products scattered in the entire lesion. Chronic lesions are also split into active and inactive groups. The active chronic lesions are enclosed in a rim of macrophages with myelin degradation products besides containing advanced level myelin degradation products in the center of the lesion, while the chronic inactive plaques are identified by a sharp border without macrophages or active microglia (Fischer et al., 2009; Kutzelnigg & Lassmann, 2014).

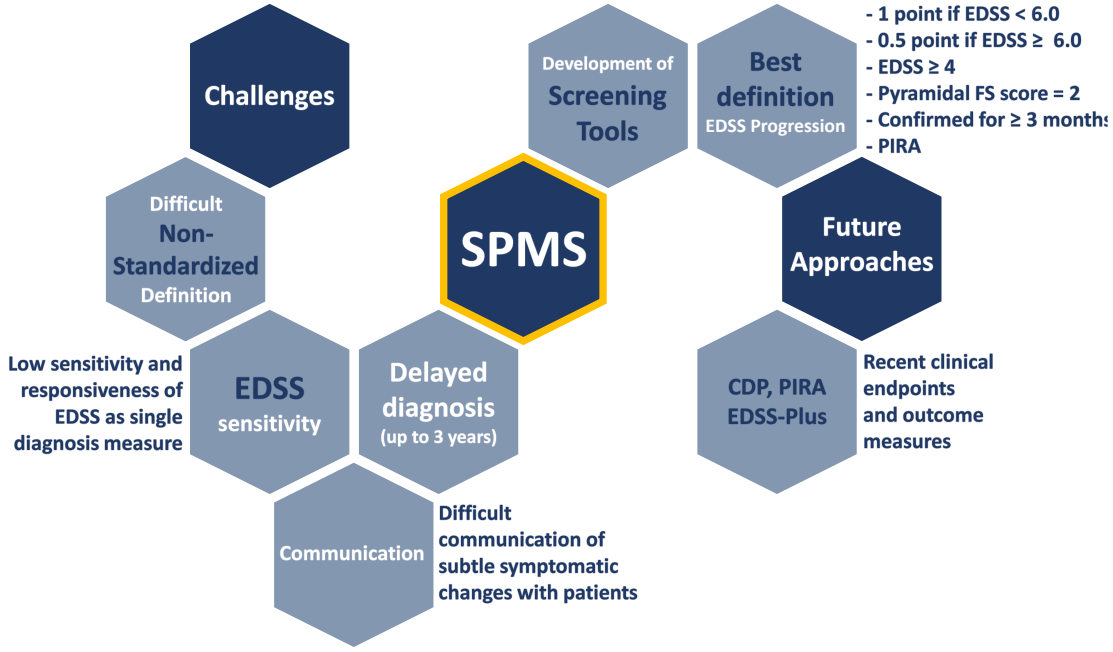

Figure 4. *Challenges and future approaches for the diagnosis and definition of SPMS Modified and reprinted from (Inojosa et al., 2019).*

RRMS is accompanied by acute lesions in WM that correlate with clinical relapses (Brück et al., 1995), whereas in SPMS the majority of the lesions are of chronic type, being either active, smoldering (slowly expanding active lesions) or inactive. Widespread and diffuse inflammation, scattered microglia activation and lymphocytes are also the characteristics, appearing throughout the WM and GM, in SPMS brains (Kutzelnigg & Lassmann, 2014; Magliozzi et al., 2010). Moreover, several in vivo imaging studies demonstrated that in SPMS brains, lesions in the low perfusion areas tend to accumulate and expand, the occurrence that is not observed in early disease levels. This phenomenon may stem from the fact that the early lesions which have formed at any site of the brain, would disappear partly due to resolution of oedema and remyelination. On the other hand, in areas exposed to low blood perfusion, early lesions persist and accumulate suggesting a stronger tissue damage (Holland et al., 2011).

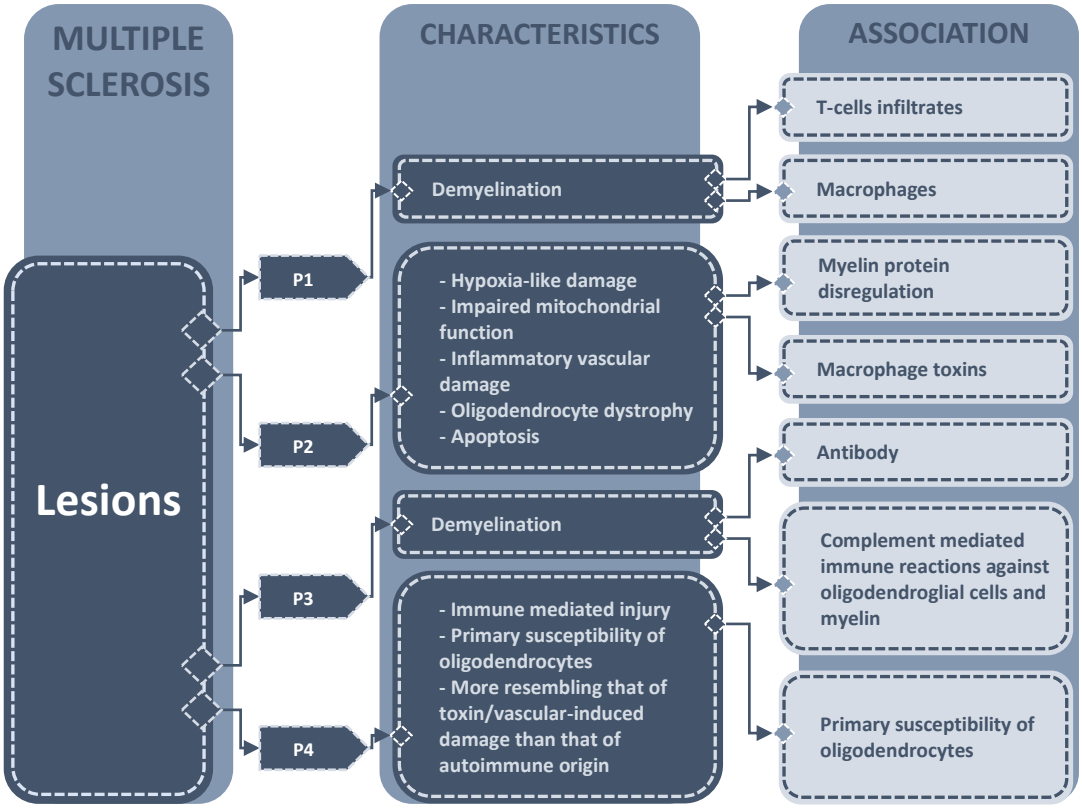

Figure 5. *Uneven distribution of hallmarks of MS lesions, leads to four patterns classification of lesions*

Modified figure inspired by manuscript of (Rissanen, 2015)

In spite of the scattered and diffuse disease markers, the intensity of TSPO binding demonstrates a gradient, varying in different sites across the subcategories of the disease (Rissanen, 2015). Different MS studies have discussed variety of brain areas with significant TSPO density due to MS, correlating to disease features such as the phenotype, disease duration and presence of relapses. These studies suggest an increasing TSPO binding in acute lesions compared to chronic plaques, elevated TSPO in scattered areas relating to demyelinating lesions, NAWM and deep gray matter such as Thalami and Brainstem, gadolinium enhanced active lesions along with non-enhancing T2 lesions in presence of relapses and in non-relapsing states, while T2 lesions in general is considered to contain similar TSPO density as of the NAWM. Considering that the TSPO upregulation and its subsequent effects show a dissimilar distribution in the CNS, MS lesions can be classified in four patterns as illustrated in Figure 5 (Rissanen, 2015).

2.5.2 Translocator protein 18kDA (TSPO) in MS studies

Therapy response and the clinical progression indicate that MS is a heterogeneous disorder. This finding is also suggested by the investigation of radiological and histopathological changes of the disease. Hence, defining the features that distinctively facilitate the diagnosis and prognosis of MS would be a key to open this mystery box. In this matter, the objectively measurable biomarkers of the disease would be an important target to identify (Filippi et al., 2012; Ziemssen et al., 2019). A biomarker (limited to imaging biomarkers in this study) as a specific index of pathological process and pharmacological reaction to therapy, is defined as an existent indicator in subjects with a certain disease, while it is absent or less significantly detected either in healthy people or in the patients with other deficits. An important peculiarity of a biomarker is the dependence of its concentration to the changes in the state of the disease, e.g., the biomarker's concentration can show consistent or contrary relation with worsening or inhibition of the disease symptoms (Ziemssen et al., 2019). In the pathological studies of MS, the translocator protein 18kDa (TSPO) as an identified marker of MS, has represented an ideal target for PET imaging of neuroinflammation *in vivo* (Venneti et al., 2006; Veronese et al., 2018).

2.6 Imaging modalities for MS study in vivo

In longitudinal monitoring of progressive MS and neuropathological studies in vivo, the use of modern neuroimaging plays a salient role in the follow up and assessment of the disease's progression. In addition, it allows non-invasive, safe, and cost-effective observation process providing advance data format that is believed to be highly promising for discovering the early driving forces and motivations of the disease onset (Russell, 2017). In contrast, the classical neuropathology either using postmortem brains or brain biopsies is not only time consuming and costly, but also not allowing an interventional and longitudinal studies (Lewis, 2002).

The in vivo pathological study of neurodegenerative disorders such as MS, requires the observation of neurophysiology of the CNS, which is closely dependent to the functional processes in the targeted areas. The quantification of such functions relies on the measurements of compound transport considering blood flow, enzymatic rates and receptor densities. The concentration of the endogenous compounds, being transformed, transported, or bound to receptors cannot be detected and quantified directly. Therefore,

injecting a tracer, concentration of which can be observed and measured via imaging tools is believed to be an effective conventional solution (Turkheimer et al., 2014). A tracer can be injected in a short bolus and accordingly the concentration's change across tissue compartments be measured in a dynamic experiment. Measurement of a tracer should follow three principles as follows:

1) The tracer should be in small portion to not to alter or perturb the system's essential functions (Phelps et al., 1979).

2) Interaction of the tracer with the system must be predictable, informative, and reproducible.

3) Tracer's concentration needs to be measured quantitatively (Turkheimer et al., 2014).

Experimental design of an in vivo study demands carefully evaluating both tracers' and imaging modalities' compliance with the above-mentioned principles.

MRI: The MR imaging data is basically a computerized outcome of the interaction between the magnetic field of the scanner and certain spinning atomic nuclei, which absorb radio frequency (RF) energy of the magnetic field. In medical and research MRI, the most commonly used nucleus is that of the Hydrogen atom within the body organs being brain and spinal in the case of brain imaging. Nuclei like hydrogen's, with odd number of protons and/or neutrons, while spinning produce a small magnetic field called magnetic moment (Hoult & Bhakar, 1997). Magnetic moment is perpendicular to the orbit axes of the nuclei and is analogous to a tiny magnet bar with north-south poles. The spinning direction of vast number of nuclei are randomly oriented and hence resulting in no magnetic field. However, being exposed to a strong external magnetic field such as that of MRI scanner the spins align to the given direction via angular momentum causing a precession at a certain rate of magnetic moment around the external magnetic field called Larmor frequency (Liney, 2006). At this stage, if a radio frequency pulse is applied, it can distort the parallel state and shift the magnetic moments away from the field. As soon as the RF pulse is suspended, the system will reform the parallel alignment with same characteristics and presence of the RF at the Larmour frequency. Through such transition, spins will release the energy received from RF pulse, a process called relaxation (Turkheimer et al.,

2014).The detectors of the scanner measure the relaxation in both forms of longitudinal (T1) and transverse (T2) during the realignment and diphase process. To obtain the MR images, the magnetic fields are to change across the tissue, imposed by the magnetic gradients. Larmor frequency varies in space allowing the signal encoding-retrievals in the field of view (Turkheimer et al., 2014).

In addition to the role of structural MRI in clinical research that enables obtaining of high-quality imaging data with excellent resolution, the possibility of tracer methodology for MR imaging, with use of compounds labelled with nuclides such as ^{13}C that can produce nuclear magnetic signals is worth to mention (Liney, 2006). However, at the moment the application of tracer methodology in functional MRI has strict limitations. The very known restriction is the low signal-to-noise ratio (SNR) that requires large concentrations of radionuclide in order to result in an adequate resolution in a proper time. Additionally, obtaining absolute quantification with use of functional MRI poses a series of difficulties that represent the MRI, as an imperfect modality for nuclear-functional imaging that does not comply the principles of tracer measurements. Therefore, pursuing tracer quantification for molecular neuropathology study is not achievable with MRI as a standalone source of observation. On the other hand, Positron Emission Tomography is the modality that suits the three principles of tracer measurement the best (Turkheimer et al., 2015).

Positron Emission Tomography: Positron emission tomography is a functional nuclear imaging technology broadly used in today's molecular and chemical neuropathology. PET imaging allows measuring of the distribution and concentration of radiopharmaceuticals inserted into an organ by calculating the annihilation photons emitted from their short-lived isotope labels such as ^{11}C, ^{18}F and ^{15}O. The ideal compliance of PET imaging with tracer measurement principles is simply stemming from the instrumentation that allows absolute quantification, nature of the target tracers that fit well in the tracer concentrations, and neutral influence of radiolabels on the tracer properties (Turkheimer et al., 2014).

The process of radiolabel isotopes production begins inside a particle accelerator called cyclotron using electromagnetic field for propelling charged particles to high velocity and energy level. The molecule is then shot into a reaction vessel usually filled with a gas mixture when the reaction between gas and the particle generates the positron emitting

isotope that is bound to the reactive molecule as what is called the 'label' (Rizzo et al., 2014; Turkheimer et al., 2014)

In positron emission tomography, the distribution of a tracer labeled with positron emitters such as ^{18}F, and ^{11}C is a fundamental parameter to be measured. The radioactivity of the PET tracer in blood and target organs is being monitored once the ligand is injected into the samples' body. The annihilation of the radiated positron with an adjacent slow-paced electron emits two γ-rays in reverse direction. The two photons will be detected as they simultaneously collide with the detector ring placed in the scanner (Gerhard, 2016; van den Hoff et al., 2014). Accordingly, the coincident detections are reconstructed in timeframes, whereas the single photon detections or signals with angles different from 180° will be considered as a noise. Meanwhile the blood sample data should be corrected for the impurities and tracer bound to red blood cells, plasma proteins etc., in order to quantify the ligand's free fraction in blood plasma (Turkheimer et al., 2015) .

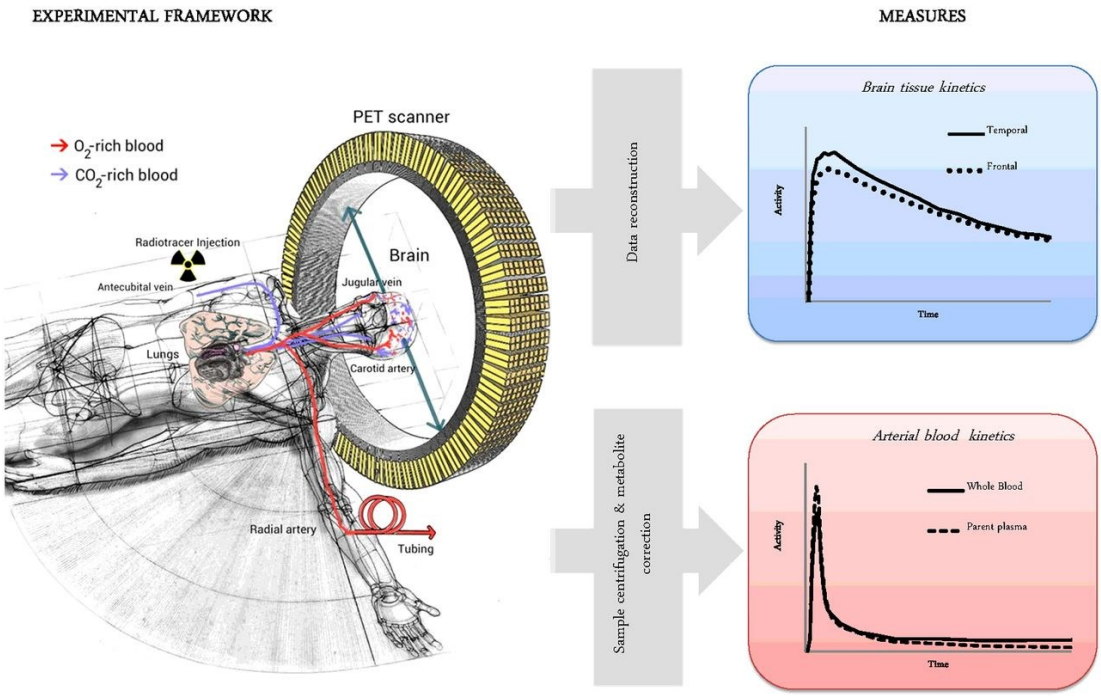

Figure 6. *Dynamic PET imaging, experimental framework, and data acquisition Reprinted from (Turkheimer et al., 2015)*

To refine the poor spatial resolution of the reconstructed images and more importantly to better addressing the location of voxels with gradient of emission in PET imaging data and relating the anatomical structure to the radioligand kinetics, the images are usually overlaid

onto corresponding slice of MR images. Hence, it is very important to consider the relativity of the spatial resolutions in MR and the PET images, since the disproportionate spatial resolution causes a disruption called Partial Volume Effect However, PVE can be corrected using various methods either during or after the image reconstruction (Carson, 2005; Erlandsson et al., 2012).

Radioligands injected into the patient's body, reach to the organ and tissue of interest via number of processes. The ligand that carries the isotope can be translocated around the body via circulatory and perfusion, transported over the membrane either actively or passively. However, it can even transport inside the cell. Chemical substances may be transformed by interference of enzymes and similar reactions, or via non-covalently combining with another partner molecule such as protein etc., to form a single complex that plays a special role in the organism target tissue (Imaizumi et al., 2008; Salmon et al., 1990; Turkheimer et al., 2015).

The physiology of the radiotracers in regions of interest (ROI) or in a target voxel is generally represented as exchanges between tissue compartments and therefore it is quantified with use of compartment modeling techniques. Compartments containing a certain quantity of a substance, may be overlapping physically since they may carry different forms of chemical species. In simplified definition, the quantification process can be explained as measuring the amount of the chemical that goes inside one compartment minus the amount that goes out of it. The concentration of the compounds is not measurable directly, so one natural solution is to inject a radiotracer with a decent binding potential to the target compound, and then monitor and track the tracer concentration and measure the process of transformation, translocation or binding of it in the target region (Tuisku et al., 2019).

In a dynamic experiment design, the tracer ligand can be injected as a short bolus and be monitored and quantified while the tracer's concentration changes across different compartment. The dynamic design allows all the exchange rates between compartments to be estimated. Nonetheless, in another form of experiment called steady-state experiment design a single measurement can be taken onward the compound reaches the equilibrium after injection (Turkheimer et al., 2015).

Compartment modeling of the radiotracer concentration is design in two common forms namely Two-Tissue 3 compartment model (2TCM) *in series* (Figure 7 A) and *parallel* simplified reference tissue model (Figure 7 B).

Kinetic analysis methods

In 2TCM compartmental model the flow state of the molecules is divided to 3 compartments of which C_0 (C_P) represents the activity concentration of the free ligand in the blood plasma before penetrating the BBB, C_1 (C_{ND}) includes lumped free ligand that inserted the BBB toward the tissue plus the amount of the radioligand that has bound to the non-specific molecules on its way to the tissue after inserting the BBB, and finally C_2 (C_B) represents the specifically bound ligand inside the target tissue. These parameters are being measured in a steady-state design along with measuring the exchange rates between these 3 stages of molecular flow when the compound reaches the equilibrium, assuming that almost all the molecules have the opportunity to transfer and exchange between the different compartments.

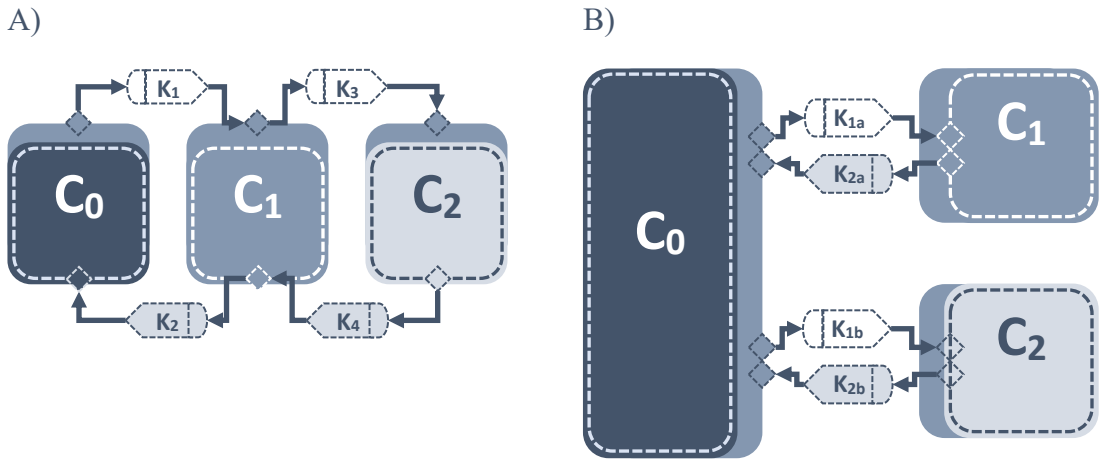

Figure 7. *A)2TCM B) Simplified reference tissue model*
Modified and reprinted from (Turku PET Centre, 2021)

The parallel model consisting of a pair of parallelly adjusted one-tissue compartment models with mutual input functions. This model is based on the assumption that the rapid kinetics of the ligand exchanging between C_1 and C_2 compared to that of the C_0 and C_2 so that the C_1 and C_2 can be combined and ROI kinetic will be calculated as a singularly (C_T) (Feng et al., 1995; Phelps et al., 1979). These two models are kinetically indistinguishable,

which can be more clearly illustrated via comparing the Time-Activity Curve simulation plots for both models on the same tissue, as the plots in Figures 8 and 9 indicating that any PET data that can fit into one model, it can be also fitted with the other.

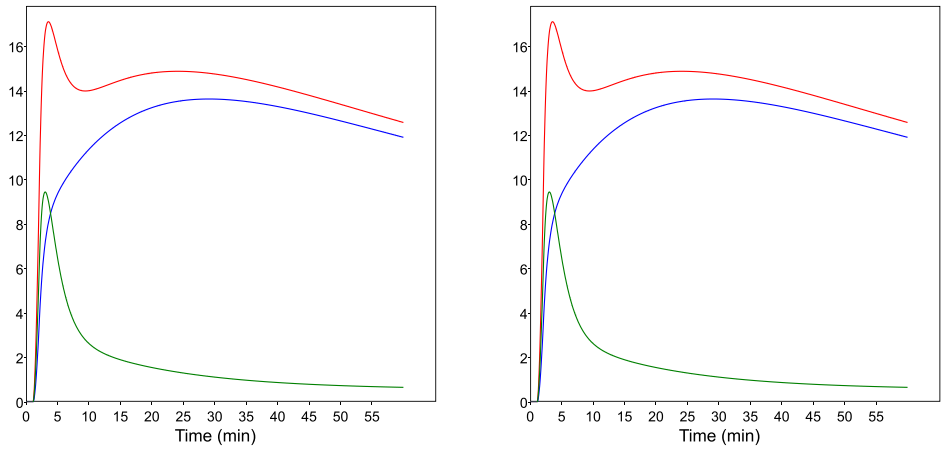

Figure 8. *"The same TAC can be simulated from the two 2TCM models (Fig. 7 A and B), using the same input function. On the left side, total tissue concentration curve (red line) is simulated using the model with tissue compartments (green and blue lines) in series. On the right side, total tissue concentration curve (red line) is simulated using the model with tissue compartments (green and blue lines) in parallel. For simplicity, contribution of blood radioactivity inside tissue vasculature is not considered in these simulations"*

Modified and reprinted from (Turku PET Centre, 2021)

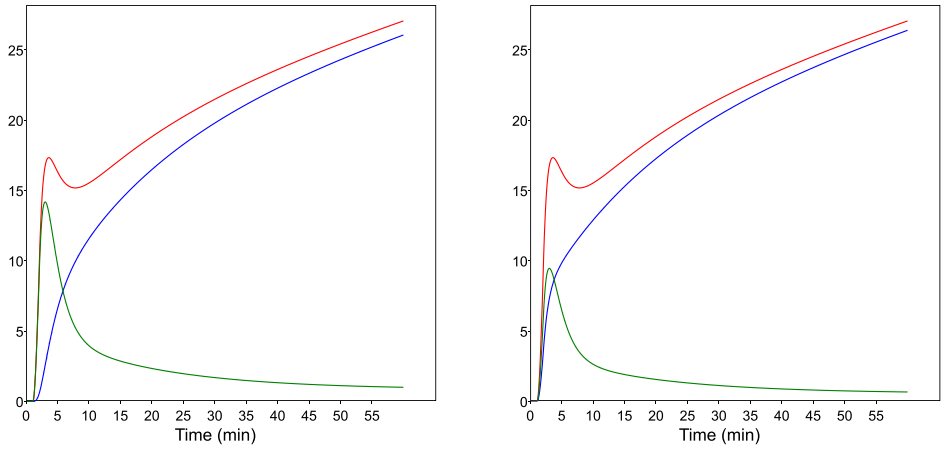

Figure 9. *"In the case of irreversible tissue uptake kinetics, the same TAC can be simulated from the two 2TCM models. On the left side, total tissue concentration curve (red line) is simulated using the model with tissue compartments (green and blue lines) in series, and with k4=0. On the right side, total tissue concentration curve (red line) is simulated using the model with tissue compartments (green and blue lines) in parallel, and with k2b=0."*

Modified and reprinted from (Turku PET Centre, 2021)

In one-tissue compartmental model the total radioactivity is calculated via augmenting the two compartments:

1) $C_T(t) = C_1(t) + C_2(t)$

In 2TCM *series* model (Figure 7 A), the concentration of the ligand can be calculated by two differential equations as follows:

2) $\frac{dC_1(t)}{dt} = K_1C_0(t) - (K_2 + K_3)C_1(t) + K_4C_2(t)$

3) $\frac{dC_2(t)}{dt} = K_3C_1(t) - K_4C_2(t)$

Whereas for the *parallel* 2TCM model (Figure 7 B), the ligands concentration curves $C_1(t)$ and $C_2(t)$ can be calculated by two identical differential equations:

4) $\frac{dC_1(t)}{dt} = K_{1a}C_0(t) - K_{2a}C_1(t)$

5) $\frac{dC_2(t)}{dt} = K_{1b}C_0(t) - K_{2b}C_2(t)$

Nonetheless, the parameters of the compartment model in each format can be transformed into the parameters of the other:

- Series – Parallel

6) $K_{1a} = \frac{K_1}{K_{2b} - K_{2a}} . (K_3 + K_4 - K_{2a})$

7) $K_{2a} = \frac{K_2 + K_3 + K_4 - \sqrt{(K_2 + K_3 + K_4)^2 - (4K_2K_4)}}{2}$

8) $K_{1b} = \frac{K_1}{K_{2b} - K_{2a}} . (K_{2a} - K_3 - K_4)$

9) $K_{2b} = \frac{K_2 + K_3 + K_4 + \sqrt{(K_2 + K_3 + K_4)^2 - (4K_2K_4)}}{2}$

- Parallel – Series

10) $K_1 = (K_{1a} + K_{1b})$

11) $K_{1a} = \frac{K_{1a}K_{2a} + K_{1b}K_{2b}}{K_{1a} + K_{1b}}$

12) $K_3 = \frac{K_{1a}K_{2b} + K_{1b}K\_2a}{K1a + K1b} + \frac{K_{2a}K_{2b} \cdot (K_{1a} + K_{1b})}{K_{1a}K_{2a} + K_{1b}K_{2b}}$

13) $K_4 = \frac{K_{2a}K_{2b}\,(K_{1a} + K_{1b})}{K_{1a}K_{2a} + K_{1b}K_{2b}}$

For quantification of the radioligand's binding, the macro-parameters calculated from the estimation of the kinetic model ratios are used, which are obtained by fitting the model equations in its TAC. One significant and vastly used microparameter, defined as a tissue to arterial plasma concentration rate constant is called a volume of distribution and is shown in short as V_T. Calculation of V_T provides a ratio of bind-specific (V_S) and non-displaceable fraction of the radiotracer (V_{ND}), and therefore, the Volume of distribution in total would be the sum of these two fractions (Morris et al., 2004).

14) $$V_T = V_S + V_{ND}$$

However, V_T is obtained with variety of efficient computational methods else than compartment modelling, such as graphical Logan plot, a linearized method in which the activity concentration in target region (C_T) and the arterial plasma concentration (C_P or C_0 in Figure 7 A) will be set in a linear equation as follows:

15) $$\frac{\int_0^t CT(s)ds}{CT(t)} = V_T \frac{\int_0^t Cp(s)ds}{CT(t)} + b$$

In this equation, after the time (t) from the administration of the radioligand, the parameter b represents a linear trend in the curve of which the slope can be calculated and presented as V_T (Logan, 2000). At the equilibrium, the quantification of the ratio of the specifically bound PET-tracer in relation with non-displaceable radioligand can be presented using the formula:

16) $$\begin{cases} 1)\, BP_{ND} = f_{ND} \frac{B_{avail}}{K_d} \\ 2)\, BP_{ND} = \frac{V_S}{V_{ND}} = \frac{V_T - V_{ND}}{V_{ND}} = \frac{V_T}{V_{ND}} - 1 = DVR - 1 \end{cases}$$

In equation (16 - 1), BP_{ND} represents the non-displaceable binding potential equals to the free fraction of the radioligand in non-displaceable compartment (f_{ND}) multiplied by the number of available receptors (B_{avail}) divided by the receptor affinity dissociation constant (K_d). Equation (16 - 2) showing the BP_{ND} equal to the volume of distribution of the specifically bound divided by the non-displaceable radioligand. transforming the equation via replacing the V_S by its origin, V_T - V_{ND}, BP_{ND} relates to the distribution volume ratio (DVR) with partial fraction decomposition obtaining $\frac{V_T}{V_{ND}} - 1$. Also, DVR is the ratio

estimate of volume of distribution in the target tissue compared to the reference area in the organ (Innis et al., 2007).

The process of obtaining the arterial input function is an inconvenient invasive approach that is not risk free and may cause further complications, beside the costly and error sensitive analysis routine. Hence, the simplified compartmental models are used based on the reference region as an input function, in order to omit the arterial input data and provide the direct estimation of the macro-parameters.

The suitable reference region selected for this purpose has to meet two important criteria, first to contain no specific radioligand binding, and second the non-displaceable distribution volume (V_{ND}) and the non-specific radioligand binding must be similar in reference region and the target ROI (Turkheimer et al., 2015). Due to heterogeneity and diffusivity of the degradation and axonal demyelination in MS, finding an anatomically consistent reference region that meets the optimum requirements is either very difficult or impossible. In this case, a supervised cluster algorithm (SVCA) can be utilized to iterate through the brain imaging data and define a cluster (Pseudo-reference region) of distinctively detected voxels in the brain which meet the similar criteria as of the ideal reference region (Yaqub et al., 2012). The algorithm is designed to examine the voxel-level distribution volume in the brain to collect a group of minimal sections in the WM of healthy controls, as well as those in the NAWM of the MS patients which meet the requirements within a determined standard deviation (SD) of the mean value of the global healthy WMs (Herranz et al., 2016).

In the absence of a proper anatomical reference tissue, obtaining a pseudo-reference cluster allows quantification of the PET tracer's distribution and the radioactivity concentration using simplified methods and less complex kinetic modeling approaches. In this study several methods of quantification have been examined initially before selecting a particular method for further analysis, which can be briefly explained as follows.

Logan graphical analysis (Logan V_T)

For analysis of the distribution volume and distribution volume ratio using Logan graphical method, having measured the Time Activity Curve (TAC) of an obtained reference source (either anatomical or in voxel-level), Logan graphical model can be applied using an equation as follows:

17) $$\frac{\int_0^t C_T(\tau)d\tau}{C_T(t)} = DVR\frac{\int_0^t C_R(\tau)d\tau + C_R(\tau)/k_2'}{CT(\tau)} + b$$

$C_R(t)$ and $C_{T(t)}$ respectively denote the activity concentration of the radioligand measured in PET imaging in the reference region and the target tissue. k_2' denotes the population averaged tissue-to-plasma flow constant (in min -1) from the reference ROI (Logan, 2000). The DVR here can be quantified as the slope of the linear allotment ($t > t^*$) in a related plot of the equation $\left(\int_0^t C_R(\tau)\,d\tau + \frac{C_R(t)}{k_2'}\right)/C_T(t)$ Versus $\left(\int_0^t C_T(\tau)\,d\tau\right)/C_T(t)$.

Standardized Uptake Volume (SUV)

Simplification of the PET study protocols is considered as a preferable approach in clinical studies, which helps reducing the scan time and avoiding the arterial cannulation. In this regard, direct utilization of the activity concentration to calculate the tissue-to-plasma ratio, tissue-to-blood or the tissue-to-reference ROI ratio is a conventionally used method. If it is possible to extract the blood activity from the image data, among the mentioned ratios, Tissue-to-blood ratio is particularly a favorable method to use in diagnostic studies. These ratios are simply called SUV ratios. SUV is a commonly used and robust PET quantifier, equal to the ratio of the tissue radioactivity concentration [kBq/mL] at time T and administered dose [MBq] of injection, compared to the body weight of the subject:

18) $$\text{SUV} = \frac{C_{PET}(T)}{Dose/Weight} = \frac{TAC}{Dose/Weight}$$

SUV in the above equation implicates the ratio of the regional radioactivity concentration in the whole body and thus the average SUV of the whole body is similar to the density of the body ($\lesssim 1$). In PET studies, a radioligand dose and the radioactivity of the tissue must be decay corrected to the same time point. Using the above-mentioned units, SUV will be presented by [g/ml].

Challenges with PET imaging in pathological MS studies in vivo

PET imaging of the brain faces a series of restrictions which may lead to underperforming results in the related studies. The process of PET imaging is highly expensive, and the invasive catheterization for arterial input function which may cause further complications,

and also there are strict ethical issues with the radiation exposure that may lead to a small sample size.

Moreover, despite the major effort on developing the new generation radioligands the ideal image quality has not been delivered so far. Such a barrier is assumed to relate to a number of obstacles such as the overintensified TSPO binding on the BBB that confuses the pathological tissues' signal. This is mainly because the proportion of the free ligand in blood plasma and near the BBB is much higher than the remaining ligand that penetrates the BBB towards the brain. A part of the latter fraction reaches the microglia and binds with the TSPO in the mitochondria after exchanging with a number of non-specific sites in its way. The signal received from the target tissue is obscured by the disproportional signal from the ligand portion that resides near the BBB. For a proper analysis, the obscured signal needs an adequate modeling to be properly identified (Rizzo et al., 2014). Other limitations and flaws are corresponding the restricted instrumentation, and unavailability of tissue reference region due to an extensive TSPO binding at BBB that masks the brain tissues(Turkheimer et al., 2015).

Last but not least, the nucleotide polymorphism in the TSPO gene variates the binding affinity in different participants which requires proper modelling and specific quantification approaches to clearly identify the genotypes in analysis. The nucleotide polymorphism leads to variation of binding affinity in second generation TSPO tracers at a population level (Owen et al., 2012). This trait categorizes the individuals to 3 groups of high affinity binders (HABs), low affinity binders (LABs), and mixed affinity binders, contributed to by one low-affinity site and one high-affinity site. The binding differences across TSPO genotypes vary due to the ligand affinity. Regarding that the PBR28 is the ligand with the highest affinity, for which the affinity difference translates in a 2:1 TSPO signal in PET images in HABs compared with MABs, the genetic stratification of the subjects is essential to be taken into account (Turkheimer et al., 2015).

Tackling such difficulties requires the implementation of methods that allow identifying of the fraction of the TSPO that specifically represents the inflammatory response due to MS. This must be performed via identifying the bind-specific radioligand in the target ROIs distinct form the free fraction in nonspecific sites within the CNS and its surroundings. Regarding the diffusivity and heterogenous characteristic of the TSPO in the MS brain, one gigantic challenge would be the limitation and flaw in quantification of the

radioligand's activity concentration. Above all, finding a robust method for measuring and determining a suitable reference region either anatomical or pseudo-reference obtained via supervised cluster algorithms is essential. In this study, the main objective is to test a group of quantification methods and kinetic modeling approaches, considering the different reference regions and behavior of the normalized data based on each of them.

3. AIMS OF THE STUDY

The overall objective of this study was to evaluate the novel quantification methods for analyzing neuroinflammation via TSPO radioligand aimed at acquiring the most robust quantification method among all. The specific aims, pursued in this study are more descriptively stated as follows:

- Analysis of the imaging data obtained from a clinical cohort with SPMS, compared to healthy controls, considering a selected TSPO polymorphism genotype.

- Evaluation and exploration of an optimal approach for analysis of the ^{11}C-PBR28 imaging in progressive Multiple Sclerosis.

4. MATERIALS AND METHODS

4.1 Study population

This study was carried out complementing the clinical examinations for MS study in Turku University Hospital (TYKS) and based on the data collected in Turku PET Centre with the initial group of 31 human participants, including 16 MS patients and 15 healthy volunteers (Figure 10). MS patients have been recruited via hospital district of southwest Finland, in addition to healthy control data, collected from control subjects that had previously enrolled at Turku PET Centre, localized in Turku university hospital campus. Ethical principles of Hospital District of Southwest Finland have been considered for examination approvals. Participants were provided with all necessary information and guidance for participation in the trial in advance and their consents have been collected (Tuisku, 2021).

Exclusion criteria for all study participants during the imaging were the detection of a current major neurological and psychiatric illness such as schizophrenia or major depression, substance abuse and drug dependency, history of a serious somatic, cognitive, or neurological deficit. Subjects with claustrophobia, pregnancy and medication for diabetes were also excluded from the initial study group. In regards with confirmation of these criteria, every subject underwent examinations, and their medical history was assessed (Tuisku et al., 2019). SPMS patients have followed certain criteria with two features, first including the definite disease with over two years since their last relapses, and second, having lesion load larger than 9 (T2 hyper intense MS-lesions) according to Barkhof criteria (Barkhof et al., 1997)

Moreover, prior to the first scan, participants were assessed for presence of metallic composite implants, prostheses in their body, pacemaker, ICD etc., due to their safety while being placed within the strong electromagnetic field inside the MRI tube. Subjects carrying any of these MRI incompatible devices/objects must be excluded from the study procedure.

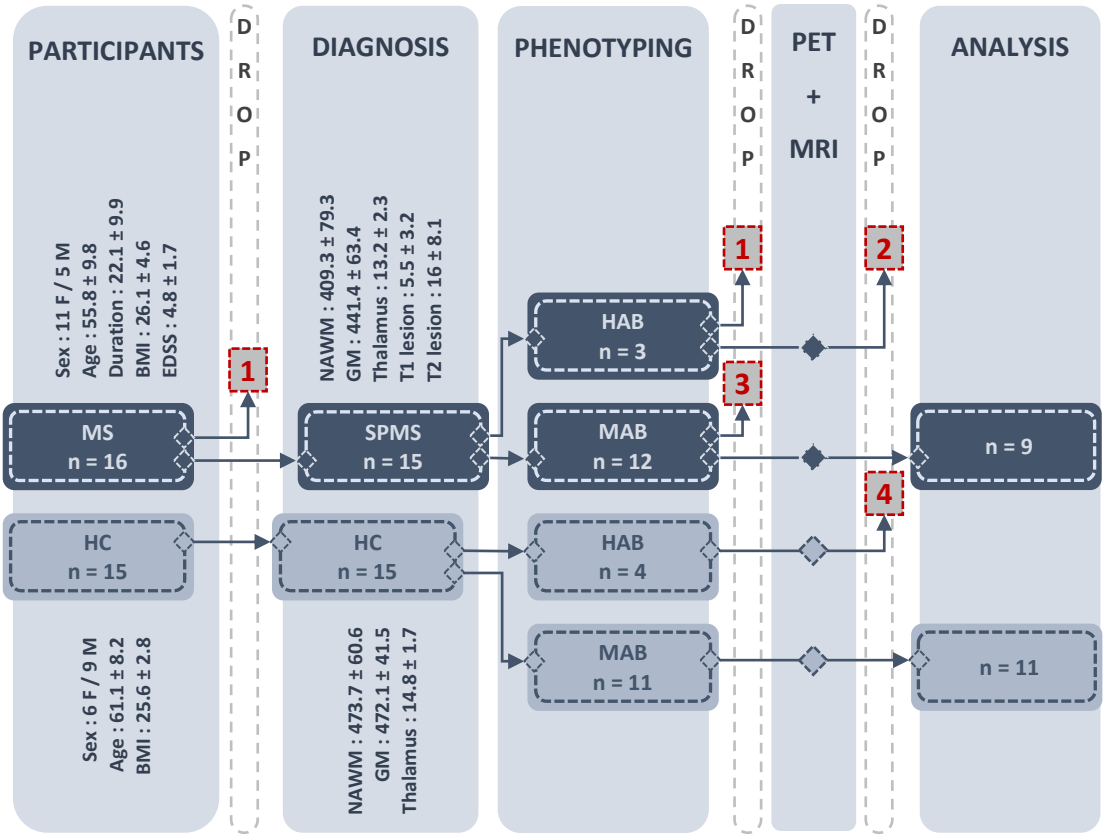

Figure 10. *Study population, Clinical characteristics, processing, and selection of the subjects. MS = Multiple Sclerosis, SPMS = Secondary progressive multiple sclerosis, HC = healthy controls, MAB = mixed affinity binders, HAB = high affinity binders, n = number*

Genotyping of the subjects were performed for the rs6971 polymorphism of the TSPO gene, classified in two major classes of mixed-affinity binders (including 13 SPMS subjects and 11 HC) and high-affinity binders (3 SPMS patients and 4 HC). Patients' background of MS treatments and diagnosis were assessed and EDSS has been measured at the baseline imaging. EDSS average in SPMS group was equal to 4.7 obtained from the group scale with minimum value of 2.0, and 7.5 at maximum. The SPMS patients' average age was 56.26 ± 8.20 years, while that of the healthy controls was 62.49 ± 8.02, indicating that the MS patients and healthy controls are not considered exactly age matched. Body mass index at baseline ranged from 18.6 to 33.6 (25.55 ± 4.34) for patients and 22.3 to 30.6 (26.19 ± 2.27) in healthy subject group (Tuisku, 2021). Descriptive statistics of subjects' clinical characteristics, demographic and MRI data are illustrated in Figure 10.

In the present study 15 MS patients have been selected with secondary progressive MS, and one patient diagnosed of RRMS (Female, age at baseline = 39) was excluded from the rest of the study. Also, the imaging data of one SPMS patient (Female, age 71.3) was

removed from the study due to its missing values and artifact in MR images. Furthermore, the data belonged to four other subjects (including 2 MABs and 2 HABs) were discarded because the PET data showed insufficient arterial information and distorted TAC content.

4.2 Data acquisition

For both healthy controls and SPMS patients, structural MR brain imaging has been performed under supervision of the study physician, aimed at exclusion of individuals with anatomical abnormalities and further delineation of the anatomical Regions of Interest for PET analysis. Accordingly, the PET imaging has been performed using ^{11}C-PBR28 radiotracer. The synthesis and also the mechanism of PET imaging performance is described complying with recently published articles from the same imaging project (Tuisku et al., 2019)

4.2.1 MR Imaging

Nowadays, not only the utilization of MR imaging is particularly important for confirming the clinical diagnosis and further monitoring of MS patients, but also the structural data obtained from MR brain imaging of subjects is an essential component in performing of a neuroradiological analysis. Subsequent assessment of lesions and normal appearing brain tissue applying Statistical Parametric Mapping (SPM/Matlab) according to brain templates and atlases are other remarkable usability of MRI data. Further, in PET analysis the PET data attenuation correction, partial volume correction, and anatomical reference region extraction is based on the corresponding co-registered brain MRI in PET/MRI studies (Rissanen, 2015; Tuisku, 2021). The data provided for the present study is obtained in Turku PET Centre utilizing 3Tesla Philips scanner for acquisition of T1-weighted scans (Philips Medical Systems, Cleveland, OH, USA). The imaging protocol included axial T1 weighted, axial T2 weighted, Coronal T2 weighted, Fluid Attenuated Inversion Recovery (FLAIR), axial Diffusion Tensor Imaging (DTI) with 16 directions and axial gadolinium-enhanced 3D T1 weighted sequences (Tuisku et al., 2019).

4.2.2 PET imaging of the MS brains

Every study subject data used in the present study was collected from the PET imaging process priorly carried out at the Turku PET Centre, utilizing the brain-dedicated, ECAT

High Resolution Research Tomography (HRRT) (CTI / Siemens, Knoxville, TN, USA), a high-resolution dual-layer crystal-detector PET scanner with 2.5 mm intrinsic spatial resolution in radial and axial directions, and almost the entire brain coverage up to level of foramen magnum due to 10 cm field of view. A flexible, individually shaped thermoplastic mask was used to minimize the head movements during the scan, alongside a Polaris Vicra motion detector device (Northern Digital Inc., Waterloo, Ontario, Canada) recording the head movements for motion tracking and quality control. The arterial catheterization was done to the right arm inserting the radialis; the injection dose of 500 MBq [3] (min. 250 MBq) was administered as a smooth intravenous bolus in less than 10 seconds at the time of injection. For attenuation correction, a 6-minute transmission scan was run utilizing the ^{137}Cs point source of the HRRT scanner after which a blood sample was taken for hematocrit assessment. Thereafter, the dynamic imaging was performed, data collection started 2 minutes before the radioligand was injected, and then the timer started at the injection moment.

PET data acquisition has been carried out in 70 minutes of resting state for each participant. PET/MR image reconstruction, frame length, arterial blood sampling and radio metabolites analysis have been decently described in recently published articles of the project which comply to protocols, previously described in the review of imaging techniques in this manuscript (Tuisku et al., 2019; Turkheimer et al., 2014).

PET images were coregistered and realigned to their corresponding MR images, also segmented into white and grey tissue classes with use of the Statistical parametric mapping toolset (SPM, version 12), running in MATLAB (The Mathworks, Natick, MA). A list of anatomical regions *(Cingulate gyrus (CIN), Caudate (CAU), Putamen (PUT), Amygdala (AMG), Insula (INS), Pallidum (PAL), VDC, Brainstem (BS), Corpus Callosum (CC), Normal Appearing White Matter (NAWM), Grey Matter cortex (GMctx), Cerebellum (CER))* were segmented using Freesurfer software (v5.3.0, Fischl, 2012) (v5.3.0, http://surfer.nmr.mgh.harvard.edu), Further, automated anatomical ROIs were generated via Automated Anatomical Labeling (AAL) *(Frontal (FRO), Parietal (PAR), Temporal (TMP), Occipital (OCC), Thalamus (THA) , Hippocampus (HIP))* onto the MR images (Tzourio-Mazoyer et al., 2002). The MR images were realigned with the summed PET images using deformation fields regarding the MRI segmentation

[3] MBq (Mega Becquerel) is the SI unit for Radioactivity

followed by multiplication of imaging data by the grey matter segment within the threshold of GM > 0.5 (Tuisku, 2021).

ROI extraction (delineation) was carried out through pursuing technical steps using T2 weighted and FLAIR MR images for identifying the T2 hyperintense lesions followed by generating the T1 hypointense lesions, semi-automatic drawing of the lesion masks and obtaining of the lesion load volumes. Next, T1 hypointense lesions were categorized into two groups, the gadolinium positive and negative, aimed at evaluating the intralesional WM ROIs and considering the two lesion sets as the core of the perilesional WM areas (Tuisku et al., 2019). A graphical roadmap for the lesion ROI extraction in WM of SPMS patients of this study is presented in the Figure 11.

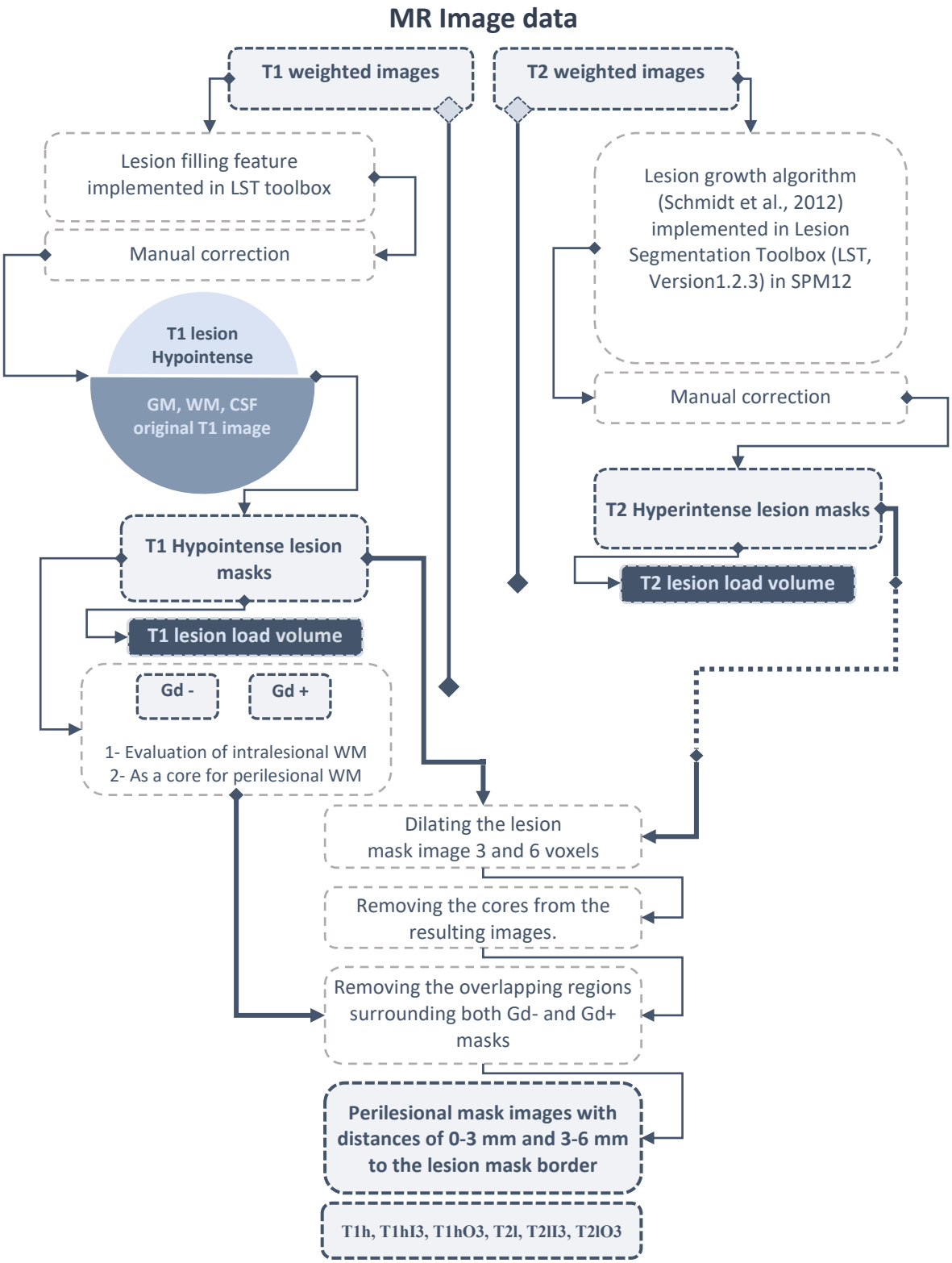

Figure 11. *The process of brain MS lesions segmentation and delineation of the ROIs has been demonstrated in this figure, performing of the coregistered PET/MR imaging data onward the preprocessing levels, using in-house software, Freesurfer (v5.3.0, Fischl, 2012) and Matlab-SPM12 (The Mathworks, Natick, MA).*

4.3 Data Analysis

In this study, the image data was pre-evaluated using semi-quantitative 3D image analysis tools such as ImageJ (Rasband & Silva, 2006). Imported into the software analysis interface, the relevant PET images were overlayed on top of the MR image. Additionally, the WM lesion areas were cropped from the image data using the corresponding slices and highlighting the lesion and perilesional area. The selected ROIs were processed for quantifying and visualizing a 3D surface plot. In the 3-dimensional plot, the heatmap and the elevated surfaces are expected to implicate the intensity of ligand concentration as it is demonstrated in the Figure 12.

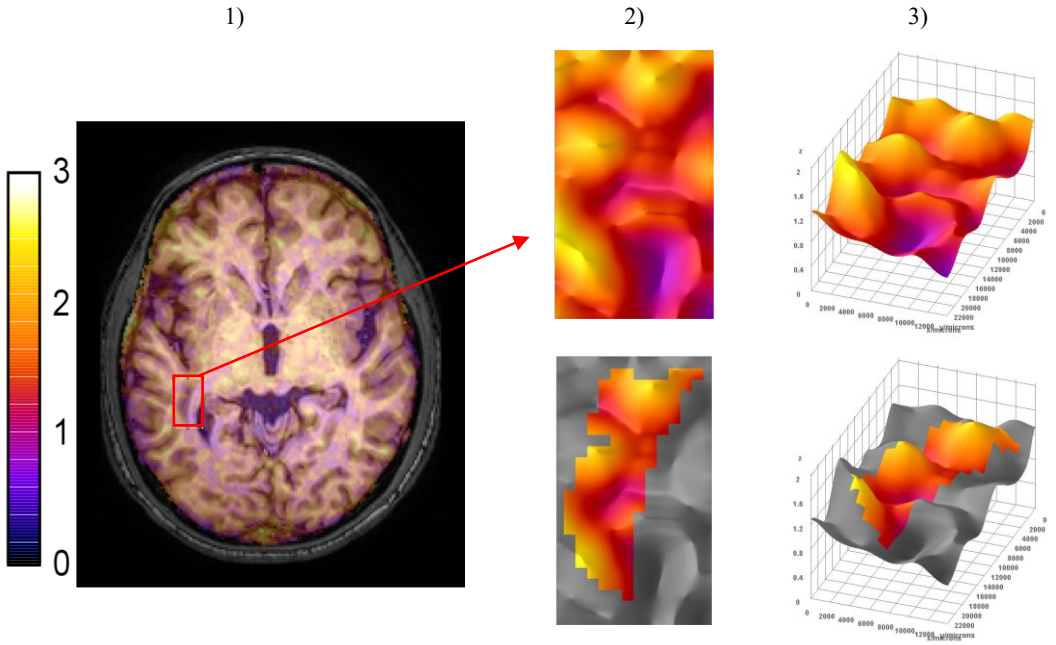

Figure 12. *3D surface plot of the MS plaque surrounding (from Turku PET Centre's MS image data). 1) PET-MR (coregistered) image, cropping the lesion and its rim within the WM, located near the temporal lobe on the right hemisphere of the patient's brain. 2) The top-down view of the plotted values of the plaque surrounding with highlighted lesion and its rim in the lower image. 3) The 3D view of the plot. The elevated surfaces represent the increasing concentration in the area, elevated surfaces are expected to be placed on the rim of the lesion as we normally expect the higher concentration on the perilesional areas while the center of the lesion is supposed to be concave due to thew presence of the dead neuronal cells which do not deliver any imaging signal.*

As is shown in the figure, the 3D visualized results illustrate a hampered valuation in the perilesional areas, which do not indicate any certain value obtained from the radioactivity concentration on the rims of the lesions. The PET images obtained from the initial values seem to not meet the expected requirements of the study for further analysis. Hence, the MR/PET imaging data required a series of modifications through a number of procedures in order to obtain a more accurate basis for data normalization and selecting a suitable reference region among the anatomical areas or via voxel-wise supervised cluster algorithm.

The quantification of the raw values from the TAC of the imaging data carried out using SPM12 and Matlab was partly done in methodology of this thesis. The quantification model and the Matlab algorithm was studied and test-modified for applying on the current data. Nonetheless, obtaining of the final values were only partly assisted under supervision of the technical advisor of this thesis. Moreover, the modification of the Supervised Clustering algorithm originally developed at Harvard University (Herranz et al., 2016) was studied, and partly assisted. Last but not least, an in-house algorithm was developed using supervised classification model in a similar manner for obtaining a pseudo-reference cluster of the brain in voxel-level, which was then discarded from this study due to inaccuracies and ineffectiveness compared to Herranz algorithm.

The following steps including the numerical data wrangling, data preparation, statistical models and analysis were all carried out utilizing a python code developed during this study (referencing Pandas, Numpy, Matplotlib, Seaborn, Stats opensource libraries).

Accordingly, The distribution concentration was compared across a list of regions, accounting the value represented by healthy controls in population level compared to those obtained from the SPMS patients data. This comparison is aimed at enabling the qualification of the different clusters of the brain, regarding the criteria for reference region selection. Among all of the regions included in this session, few of them showed the similar perfusion characteristic as the target tissues, similarity in the biomarker concentration in both patients and controls, while showing much lower specific binding with the radioligand molecules (Figure 13).

Values obtained in different anatomical segments of the brain in addition to those of the target ROIs were normalized across the values in the selected reference regions. Subsequently, the average normalized content was visualized in scatter matrices to demonstrate the correlation of the different reference regions for normalization bases.

The Partial Volume Effect (PVE) in co-registered MR and PET images is caused by binding differences between the adjacent ROIs and also by increased binding of the radiotracer in the non-specific binding sites around the cortical area. The PVE was corrected using the Geometric Transfer Matrix (GTM) method for all activity curves (Roussel et al., 1998). The distribution volume (V_T) was quantified also using Multilinear Analysis-1 (Ma1) alongside Logan graphical methods, as well as SUV was re-obtained via

the equations that are previously mentioned in the literature review. Distribution volume and standardized uptake value ratios were quantified in the same manner as the previous step, preparing the values for further level analysis.

Finally, The 2-Tissue compartmental modeled data was quantified and processed onward all of other data in previous approaches. Ratios including the Distribution Volume Ratios (DVR) of the same regions based on four selected reference regions (CER, OCC, Href, GMctx) and the constant exchange rate of the ligand (K_1) outside and inside of the tissue compartment were delivered. The voxel-level pseudo-reference region was obtained via modified version of Herranz supervised cluster algorithm in Matlab concluding DVR and SUVR with significance threshold at $P < 0.05$ (Herranz et al., 2016). The comparison of the distribution concentration between different tissues were visualized using Python programming frameworks and algorithm for data analysis (Pandas, Matplotlib, Numpy, Seaborn)

4.4 Statistical methods

In the demographic table in the results section, all comparisons and MRI metrics have been demonstrated as means and standard deviations. The results of the demographic comparisons are shown with t-test p-value and have been marked with * in case of significance.

Using the selected final method demonstrated in this study, being the 2TCM compartmental modeled logan V_T, the ligand's distribution concentration has been compared between healthy controls and SPMS patients first in three anatomical regions showing the most concentration activity in the initial evaluations and also previous studies (Sucksdorff et al., 2020; Tuisku et al., 2019). Additionally, K1 perfusion constant ratio between the free ligand in the blood plasma before penetrating the BBB and the second compartment placed after the BBB before the specific binding tissue, has been accounted for a general investigation. Accordingly, the constant ratio and the DVR have been considered in the statistical model, using python programming language. The independent T-test P-value was validated and annotated on the visualized comparison plots using Seaborn and Statannot.

5. RESULTS

Participants' demographic information, MR Imaging and clinical data and TSPO binding genotypes are illustrated in Table 2. Though the two groups are not completely matched in BMI and age, their differences are not significant. The proportion of the female population is higher among the SPMS patients than the controls, as the 7 females versus 2 male SPMS patients are included in the study, whereas 3 females versus 8 male subjects participated as healthy controls. The long duration of the disease in SPMS subjects is associated with EDSS grade 3 and above averaged around 4.72. In healthy controls' MRI content, GM cortex mean volume is quite close to the normal appearing WM, whereas in SPMS subjects the difference between the same parameters is considerable. Also, the descriptive statistic and t-test *p*-value represent a significantly lower average volume in the cerebral NAWM, Thalamus and cortical GM of SPMS patients compared to those of the healthy participants.

Table 2. *Demographics and clinical characteristics (mean [SD])*

	Controls (n = 11)	**SPMS (n=9)**	**SPMS vs. HC**
Gender (F/M)	3/8	7/2	*F/M* * $_{(P<.05)}$
Age (years)	62.66 ± 8.50	56.26 ± 8.69	*P > .05*
BMI	26.98 ± 2.38	25.51 ± 4.64	*P > .05*
Disease duration	--	20.64 ± 5.91	
EDSS	--	4.72 ± 1.77	
Genotype	MAB	MAB	
MRI metrics (mean [SD])			
NAWM volume	478.32 ± 60.35	381.88 ± 63.98	* *P < .05*
GM volume	475.52 ± 40.39	418.04 ± 50.41	* *P < .05*
Thalamus volume	14.82 ± 1.74	13.04 ± 2.04	* *P < .05*
all T1 lesion	--	5.52 ± 3.96	
all T2 lesion	--	15.07 ± 9.52	

Demographic, MRI, and clinical characteristics of the study subjects. Proportion of the Female population is calculated via calculation of the standard error referred to the 'standard normal Z distribution table'. Age, BMI and the MRI metrics have been compared between the two groups, using independent t-test with the significance threshold of <.05

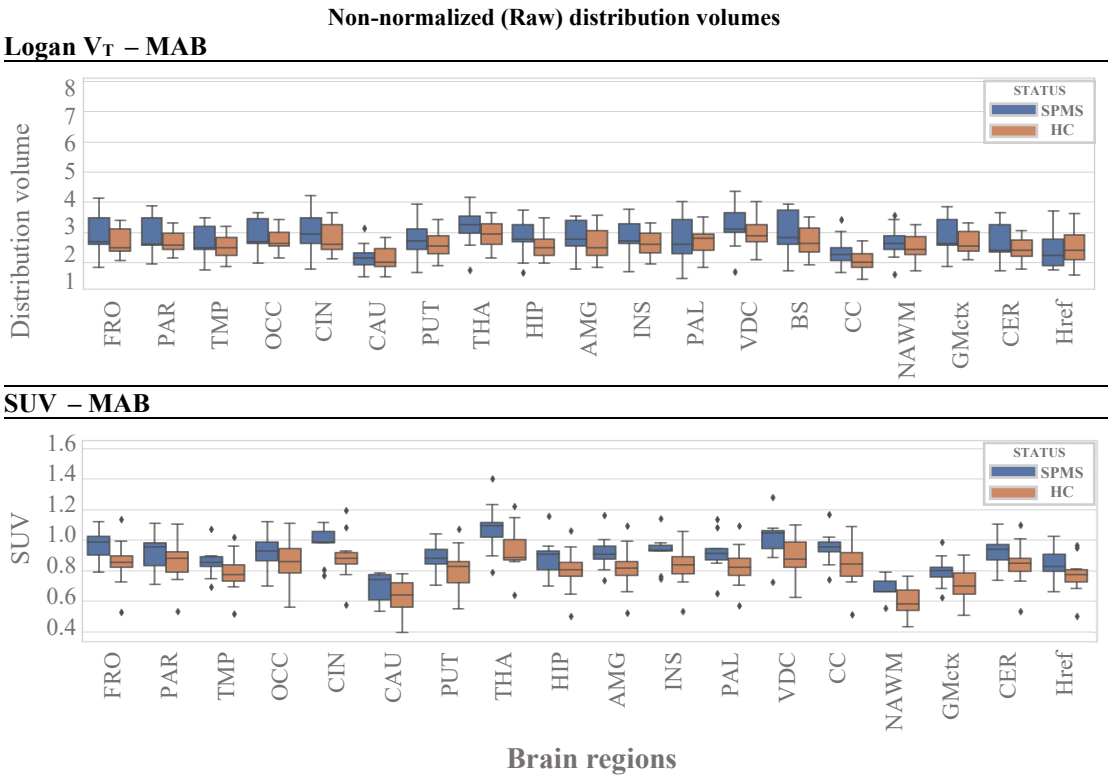

Figure 13. *Comparing the distribution concentration (Logan VT and SUV) measured in the anatomical regions and the pseudo-reference. The plot represents the VT as the preferable parameter, also suggest caudate, cerebellum, occipital, grey matter cortex and Href as the best suiting references in the further analysis.*

VT = Volume of Distribution, SUV = Standardized Uptake Value, MAB = Mixed Affinity Binders, SPMS = Secondary Progressive Multiple Sclerosis, HC = Healthy Control

As mentioned in the methodology section, for enabling of the quantification of different reference clusters in the brain at voxel level, we compared a list of regions according to the distribution concentration, obtained from the SPMS subjects over that of the HCs. A short number of the regions implied similar perfusion while representing lower specific binding with the radiotracer molecules (Figure 13).

Differences of the samples in each step of the study, illustrated in form of boxplots have been examined with independent t-test. The comparison of the raw data in scatter matrices is demonstrated with Spearman correlation (rho (ρ)), ' in the upper orthogonal sections of the matrix (Figure 14).

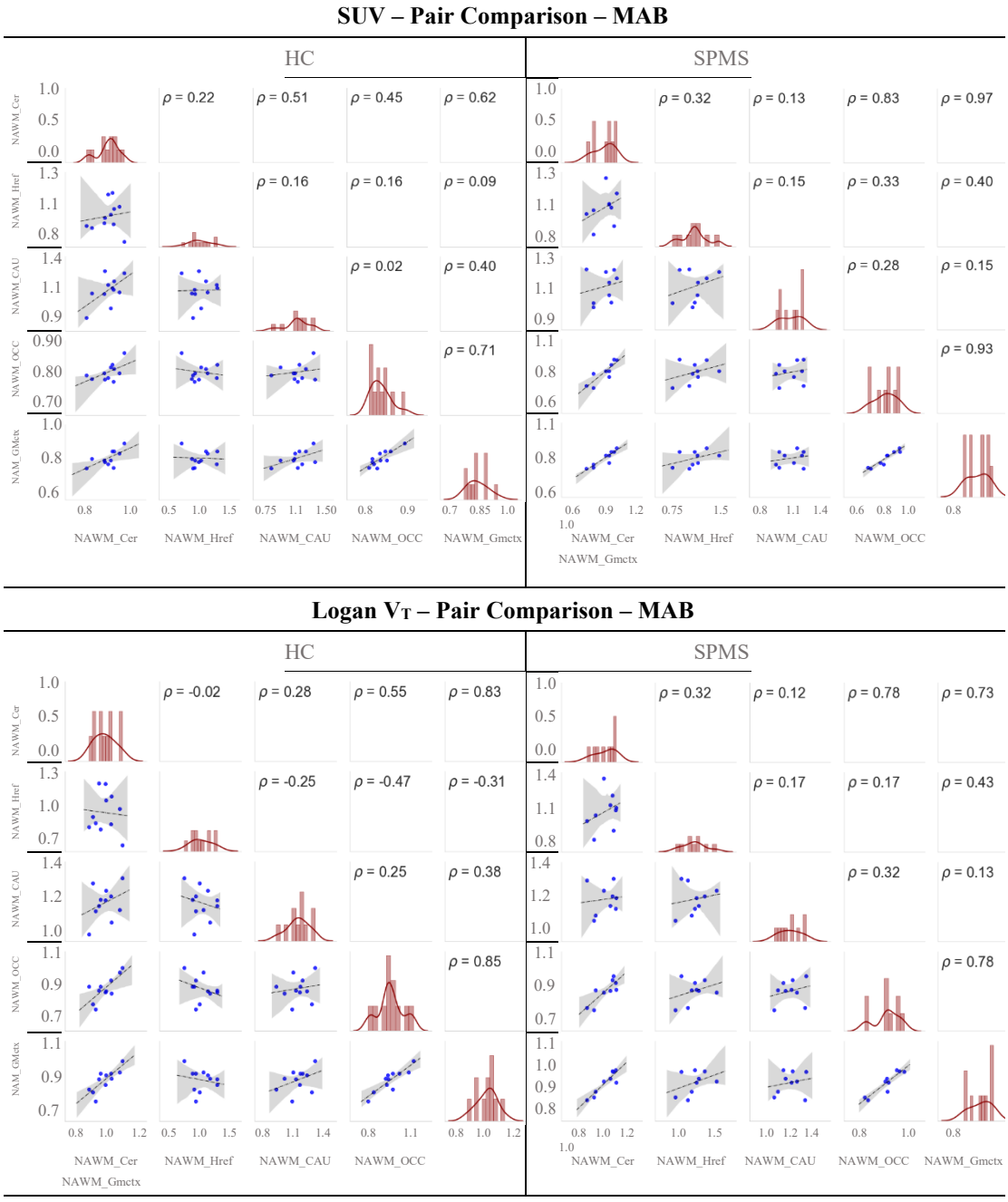

Figure 14. *The scatter matrices provided an initial comparison between the different reference regions (Grey Matter cortex (GMctx), Cerebellum (Cer), Caudet (CAU), Occipital (OCC), Herranz Supervised Cluster reference region (Href)) suggestive for selecting the most adequate references among all (Herranz et al., 2016)*

VT = Volume of Distribution, SUV = Standardized Uptake Value, PVC = Partial Volume Correction, MS = Multiple Sclerosis, HC = Healthy Control, ns = Not Significant

The non-normalized data examined at this stage was taken into account before and after the Partial Volume Correction with GTM method and showed null result when comparing the distribution concentration of the two sample groups. The K1 constant ratio for the partial volume corrected data related to Thalamus shows a significant difference between the two groups of HC and SPMS. However, this parameter does not deliver any finding in favor of the aim of this study (Figure 15).

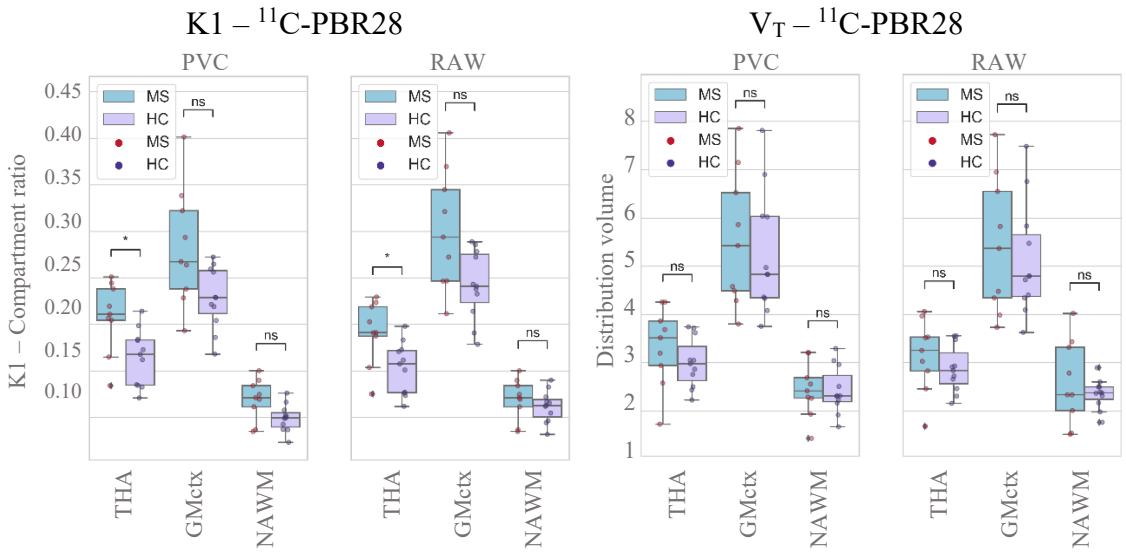

Figure 15. *2TCM - 11C-PBR28, Thalamus, GM cortex, Normal appearing WM*
Non-normalized data after applying the 2TCM kinetic model has been examined considering the three selected ROIs (Thalamus, NAWM, GMctx), compared between healthy control participants and the SPMS patients. (The entire final sample is from MAB polymorphism genotype group).

K1 = The perfusion rate constant of the free plasma ligand before and after the BBB, VT = Volume of Distribution, PVC = Partial Volume Correction, MS = Multiple Sclerosis, HC = Healthy Control, ns = Not Significant

The null result at this stage is the motivation for further analysis of the data after normalization based on the selected reference ROIs *(CER, GMctx, OCC)* and the pseudo-reference cluster *(Href)*. Nonetheless, the volume of distribution did not show any significant difference in any of the target regions *(Thal, GMctx, NAWM)*, on any normalization bases *(CER, OCC, GMctx, Href)*. In the normalized case, K1 parameter showed higher amount in the normal white matter, normalized on basis of cerebellum and GMctx reference regions, for HC brain average ratio compared to the SPMS brains (Figure 16).

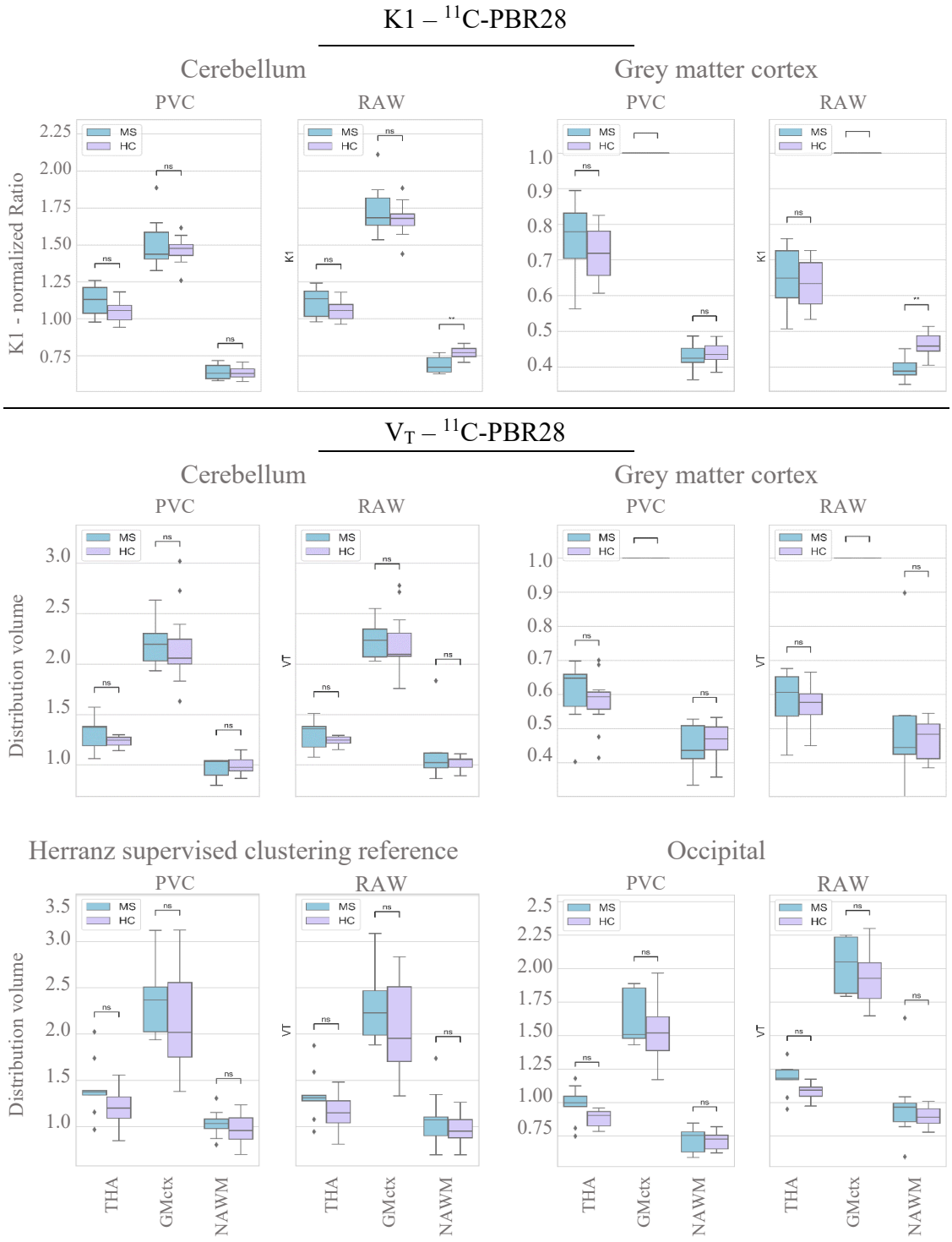

Figure 16. *Normalized 2TCM - 11C-PBR28, Thalamus, GM cortex, Normal appearing WM K1 shows a higher dynamic in Healthy brains' data than those of the MS patients. Normal appearing WM values normalized based on Cerebellum and GMctx. Volume of Distribution VT yet does not show significant difference in neither of the selected ROIs and selected reference.*

K1 = The perfusion rate constant of the free plasma ligand before and after the BBB, VT = Volume of Distribution, PVC = Partial Volume Correction, MS = Multiple Sclerosis, HC = Healthy Control, ns = Not Significant

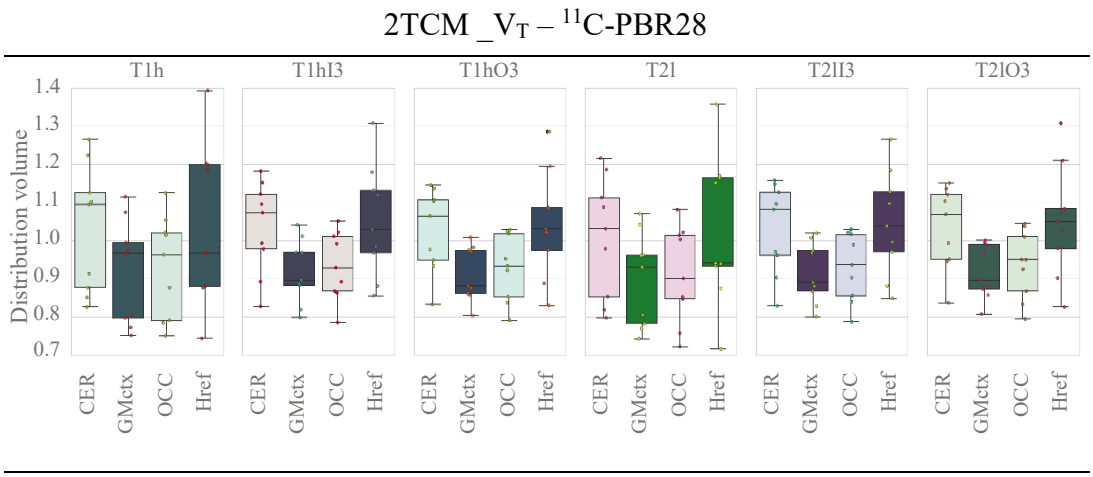

Figure 17. *No partial volume corrected but normalized 2TCM_VT, in WM lesions and perilesional ROIS. Each box represents the value corresponding the target ROI mentioned in the plot header, normalized based on the reference region denoted below the box.*

2TCM = 2 Tissue – 3 Compartmental model, T1h = T1 hypointense lesions, T1hI3 = T1 lesions' 0-3mm inner rim, T1hO3= T lesions' 1 3-6mm outer rim, T2l = T2 hyperintense lesions, T2lI3 = T2 lesions' 0-3mm inner rim, T2lO3 = T2 lesions' 3-6mm outer rim

The volume of distribution quantified via the 2TCM compartmental model and no PVC imaging data, shown in the Figure 17, represents the volume of distribution of the radioligand on the SPMS brains white matter lesion areas and the perilesional rims segmented using T1 and T2 weighted MR images of the MS brains. The higher concentration volume of the tracer bound TSPO, is expected to be observed in the edge of chronically active lesions (T1hI3, T1hO3, T2lI3, T2hO3) representative of microglial activation. Though, the visualized data here indicates a slightly higher values in the lesion ROIs and the perilesional areas when the parameters are normalized based on cerebellum and Href pseudo-reference regions, the significance of the differences still does not meet the expected criteria of support for the study's hypothesis.

6. DISCUSSION AND CONCLUSION

This study aims to find a robust mathematical method for quantification of the activity concentration of the radioligand ^{11}C-PBR28, a bind specific radiotracer to the TSPO which is found to be a biomarker of the neuroinflammation, and microglia activation observed in the Multiple Sclerosis pathological in vivo studies. ^{11}C-PBR28 is a second-generation radiotracer recently used for PET imaging of the nervous system, aimed at compensating the shortcomings that have been existed for more than 2 decades during PET analysis with use of the most conventional PET-tracer ^{11}C-PK11195.

The PET imaging data implemented in this study has been preprocessed and coregistered to the corresponding MRI data beforehand. TAC of brain regions were calculated after ROI segmentation and lesion delineation, using free surfer and SPM12. Thereafter the ligand activity concentration was estimated obtaining volume of distribution (delivered via Logan method and Ma1) in addition to the standardized uptake value. Accordingly, it has been tried to pre-examine the imaging data acquired from SPMS and healthy controls who underwent the PET-MR brain imaging, utilizing ^{11}C-PBR28 radioligand. Subsequently, several models of quantification of the microglia activation were investigated by statistically comparing the tracer's distribution concentration in different anatomical regions of the SPMS brain against those of the healthy controls. Finally, we narrowed down the number of the test-regions while also selecting a short list of the reference areas in the brain hypothesized as the most probable effective references, with a certain criteria of qualification. Additionally, a voxel level cluster obtained via modified algorithm in MATLAB has been accounted as the supervised clustering pseudo-reference to cover up lacking an effective anatomical reference region that stems from lack of the clear signal from the target tissue (Herranz et al., 2016).

The primary estimates via boxplots using t-test and scatter matrices using spearman's correlation coefficient, led to selecting a short list of regions considered for the normalization bases of the value quantification (Figure 13 and 14). Subsequently, the group comparison of the three main regions (Thalamus, NAWM, GMctx) before and after the normalization of the data was performed which did not deliver a significant finding.

Nonetheless, neither of the examined methods delivered a significant result to justify the higher activity concentration of the disease biomarker in the affected areas including

perilesional rims of the chronically active and slowly growing lesions, a hypothesis that is broadly suggested by the previously published MS studies (Airas et al., 2015; Sucksdorff et al., 2020; Tuisku et al., 2019). Though, in the present study most of the possible methods for kinetic modeling and quantification of the distribution concentration of the ligand were tested in the primary steps, 2TCM compartmental modeled data was selected for analysis as the most probably robust model. Should be mentioned that Partial Volume Correction was performed for the imaging data used in every model applied in this study, though the data was analyzed both with and without PVE.

In the traditional PET studies using ^{11}C-PK11195, the unknown localization of the microglial activation and the abnormal TSPO density exposure throughout the nervous system are believed to be the most important challenges preventing the use of an anatomical reference region, either using a supervised cluster analysis to extract the reference TAC as an alternative input function instead of the blood plasma concentration (Betlazar et al., 2018; Imaizumi et al., 2008; Turkheimer et al., 2015).

However, the second-generation radiotracers have not ideally improved the flaws of the ^{11}C-PK11195, especially about the poor signal to noise ratio and binding specificity shortcomings. Moreover, the dependency of the second generation radioligand to the nucleotide polymorphism in the 18kDA gene (rs6971) that classifies the binding affinity of the TSPO tracers in a sample group (HAB, MAB, LAB), could be considered as another main challenge for delivering a strong result that is not hampered by the diversity of the binding at the population level (Turkheimer et al., 2015). PET-MR imaging studies are usually carried out with a small sample groups due to many limitations such as the ethical protocols for radiation exposure, cost, and the invasive and inconvenient catheterization for acquiring the blood plasma input data. The latter challenge being the polymorphism genotyping of the sample cohorts, even squeezes the data size more, if not causing any total data dropouts (Tuisku et al., 2019). In this study, the initial sample cohort consisting of 16 MS patients and 15 healthy controls, has dismissed 7 patients, and 4 controls, among which 2 SPMS and 4 HC were dropped out because of the different genotype polymorphism and the hampered result was delivered from those samples' TAC data.

Data acquisition in a sample cohort with a larger size is obviously an advantage for obtaining stronger results. Moreover, regarding the challenges with variety of methods in this study leading to a null result, accounting the blood plasma concentration input function as reference could be a possible suggestion which may reconcile or improve the current

finding by providing the study with more reliable bases for the quantification of the distribution concentration of the radioligand.

7. REFERENCES

Airas, L., Rissanen, E., & Rinne, J. O. (2015). Imaging neuroinflammation in multiple sclerosis using TSPO-PET. *Clinical and Translational Imaging*, *3*(6), 461–473. https://doi.org/10.1007/s40336-015-0147-6

Anderson, A. N., Pavese, N., Edison, P., Tai, Y. F., Hammers, A., Gerhard, A., Brooks, D. J., & Turkheimer, F. E. (2007). A systematic comparison of kinetic modelling methods generating parametric maps for [11C]-(R)-PK11195. *NeuroImage*, *36*(1), 28–37. https://doi.org/10.1016/j.neuroimage.2007.02.017

Ascherio, A., & Munger, K. L. (2010). Epstein-barr virus infection and multiple sclerosis: A review. *Journal of Neuroimmune Pharmacology*, *5*(3), 271–277. https://doi.org/10.1007/s11481-010-9201-3

Barkhof, F., Filippi, M., Miller, D. H., Scheltens, P., Campi, A., Polman, C. H., Comi, G., Ade`r, H. J., Losseff, N., & Valk, J. (1997). Comparison of MRI criteria at first presentation to predict conversion to clinically definite multiple sclerosis. *Brain*, *120*, 2059–2069.

Batarseh, A., & Papadopoulos, V. (2010). Regulation of translocator protein 18kDa (TSPO) expression in health and disease states. *Molecular and Cellular Endocrinology*, *327*(1–2), 1–12. https://doi.org/10.1016/j.mce.2010.06.013

Betlazar, C., Harrison-Brown, M., Middleton, R. J., Banati, R., & Liu, G. J. (2018). Cellular sources and regional variations in the expression of the neuroinflammatory marker translocator protein (TSPO) in the normal brain. *International Journal of Molecular Sciences*, *19*(9), 1–18. https://doi.org/10.3390/ijms19092707

Bezzini, D., & Battaglia, M. A. (2017). Multiple sclerosis epidemiology in Europe. In *Advances in Experimental Medicine and Biology* (Vol. 958, pp. 141–159). Springer New York LLC. https://doi.org/10.1007/978-3-319-47861-6_9

Brück, W., Porada, P., Poser, S., Rieckmann, P., Hanefeld, F., Kretzschmarch, H. A., & Lassmann, H. (1995). Monocyte/macrophage differentiation in early multiple

sclerosis lesions. *Annals of Neurology*, *38*(5), 788–796. https://doi.org/10.1002/ANA.410380514

Carson, R. E. (2005). Tracer Kinetic Modeling in PET. *Positron Emission Tomography*, 127–159. https://doi.org/10.1007/1-84628-007-9_6

Chauveau, F., Boutin, H., van Camp, N., Dollé, F., & Tavitian, B. (2008). Nuclear imaging of neuroinflammation: A comprehensive review of [11C]PK11195 challengers. In *European Journal of Nuclear Medicine and Molecular Imaging* (Vol. 35, Issue 12, pp. 2304–2319). https://doi.org/10.1007/s00259-008-0908-9

Chen, M. K., & Guilarte, T. R. (2008). Translocator protein 18 kDa (TSPO): molecular sensor of brain injury and repair. *Pharmacology & therapeutics*, *118*(1), 1–17. https://doi.org/10.1016/j.pharmthera.2007.12.004

Compston, A., & Coles, A. (2008). Multiple sclerosis. *The Lancet*, *372*(9648), 1502–1517. https://doi.org/10.1016/S0140-6736(08)61620-7

Costello, K., Halper, J., Kalb, R., Skutnik, L., & Rapp, R. (2014). THE USE OF DISEASE-MODIFYING THERAPIES IN MULTIPLE SCLEROSIS - Principles and Current Evidence. *Multiple Sclerosis Coalition*. https://www.nationalmssociety.org/NationalMSSociety/media/MSNationalFiles/Brochures/DMT_Consensus_MS_Coalition.pdf

Delforge, J., Syrotam Andre, & Bendriem, B. (1996). Concept of reaction volume in the in vivo ligand-receptor model. *The Journal of Nuclear Medicine*, *37*(1), 118–125.

DiSabato, D. J., Quan, N., & Godbout, J. P. (2016). Neuroinflammation: the devil is in the details. *Journal of Neurochemistry*, *139*, 136–153. https://doi.org/10.1111/jnc.13607

Erlandsson, K., Buvat, I., Pretorius, P. H., Thomas, B. A., & Hutton, B. F. (2012). A review of partial volume correction techniques for emission tomography and their applications in neurology, cardiology and oncology. *Physics in Medicine & Biology*, *57*(21), R119. https://doi.org/10.1088/0031-9155/57/21/R119

Feng, D., Ho, D., Chen, K., Wu, L. C., Wang, J. K., Liu, R. S., & Yeh, S. H. (1995). An Evaluation of the Algorithms for Determining Local Cerebral Metabolic Rates of Glucose Using Positron Emission Tomography Dynamic Data. *IEEE Transactions on Medical Imaging*, *14*(4), 697–710. https://doi.org/10.1109/42.476111

Filippi, M., Rocca, M. A., Barkhof, F., Brück, W., Chen, J. T., Comi, G., DeLuca, G., de Stefano, N., Erickson, B. J., Evangelou, N., Fazekas, F., G Geurts, J. J., Lucchinetti, C., Miller, D. H., Pelletier, D., Gh Popescu, B. F., & Lassmann, H. (2012). Association between pathological and MRI fi ndings in multiple sclerosis. *Lancet Neurol*, *11*, 349–360. www.thelancet.com/neurology

Fischer, M., Raabe, T., Heisenberg, M., & Sendtner, M. (2009). Drosophila RSK negatively regulates bouton number at the neuromuscular junction. *Developmental Neurobiology*, *69*(4), 212–220. https://doi.org/10.1002/DNEU.20700

Gerhard, A. (2016). TSPO imaging in parkinsonian disorders. *Clinical and Translational Imaging*, *4*(3), 183–190. https://doi.org/10.1007/s40336-016-0171-1

Gerhard, A., Pavese, N., Hotton, G., Turkheimer, F., Es, M., Hammers, A., Eggert, K., Oertel, W., Banati, R. B., & Brooks, D. J. (2006). In vivo imaging of microglial activation with [11C](R)-PK11195 PET in idiopathic Parkinson's disease. *Neurobiology of Disease*, *21*(2), 404–412. https://doi.org/10.1016/j.nbd.2005.08.002

Ghasemi, N., Razavi, S., & Nikzad, E. (2016). Multiple Sclerosis: Pathogenesis, Symptoms, Diagnoses and Cell-Based Therapy. *cell journal*, *19*(1), 1–10. https://doi.org/10.22074/cellj.2016.4867

Ginhoux, F., Lim, S., Hoeffel, G., Low, D., & Huber, T. (2013). Origin and differentiation of microglia. In *Frontiers in Cellular Neuroscience* (Issue MAR). https://doi.org/10.3389/fncel.2013.00045

Gross, H. J., & Watson, C. (2017). Characteristics, burden of illness, and physical functioning of patients with relapsing-remitting and secondary progressive multiple sclerosis: a cross-sectional US survey. *Neuropsychiatric Disease and Treatment*, *13*, 1349–1357. https://doi.org/10.2147/NDT.S132079

Haider, L., Zrzavy, T., Hametner, S., Höftberger, R., Bagnato, F., Grabner, G., Trattnig, S., Pfeifenbring, S., Brück, W., & Lassmann, H. (2016). The topograpy of demyelination and neurodegeneration in the multiple sclerosis brain. *Brain*, *139*(3), 807–815. https://doi.org/10.1093/brain/awv398

Herranz, E., Giannì, C., Louapre, C., Treaba, C. A., Govindarajan, S. T., Ouellette, R., Loggia, M. L., Sloane, J. A., Madigan, N., Izquierdo-Garcia, D., Ward, N., Mangeat, G., Granberg, T., Klawiter, E. C., Catana, C., Hooker, J. M., Taylor, N., Ionete, C., Kinkel, R. P., & Mainero, C. (2016). Neuroinflammatory component of gray matter pathology in multiple sclerosis. *Annals of Neurology*, *80*(5). https://doi.org/10.1002/ana.24791

Holland, C. M., Charil, A., Csapo, I., Liptak, Z., Ichise, M., Khoury, S. J., Bakshi, R., Weiner, H. L., & Guttmann, C. R. G. (2011). *The Relationship between Normal Cerebral Perfusion Patterns and White Matter Lesion Distribution in 1 , 249 Patients with Multiple Sclerosis*. *80*, 129–136. https://doi.org/10.1111/j.1552-6569.2011.00585.x

Hoult, D. I., & Bhakar, B. (1997). NMR signal reception: Virtual photons and coherent spontaneous emission. *Concepts in Magnetic Resonance*, *9*(5), 277–297. https://doi.org/10.1002/(sici)1099-0534(1997)9:5<277::aid-cmr1>3.0.co;2-w

Imaizumi, M., Briard, E., Zoghbi, S. S., Gourley, J. P., Hong, J., Fujimura, Y., Pike, V. W., Innis, R. B., & Fujita, M. (2008). Brain and whole-body imaging in nonhuman primates of [11C]PBR28, a promising PET radioligand for peripheral benzodiazepine receptors. *NeuroImage*, *39*(3), 1289–1298. https://doi.org/10.1016/j.neuroimage.2007.09.063

Innis, R. B., Cunningham, V. J., Delforge, J., Fujita, M., Gjedde, A., Gunn, R. N., Holden, J., Houle, S., Huang, S.-C., Ichise, M., Iida, H., Ito, H., Kimura, Y.,

Koeppe, R. A., Knudsen, G. M., Knuuti, J., Lammertsma, A. A., Laruelle, M., Logan, J., … Carson, R. E. (2007). Consensus nomenclature for in vivo imaging of reversibly binding radioligands. *Journal of Cerebral Blood Flow & Metabolism*, *27*, 1533–1539. https://doi.org/10.1038/sj.jcbfm.9600493

Inojosa, H., Proschmann, U., Akgün, K., & Ziemssen, T. (2021). A focus on secondary progressive multiple sclerosis (SPMS): challenges in diagnosis and definition. *Journal of Neurology*, *268*(4), 1210–1221. https://doi.org/10.1007/s00415-019-09489-5

Kamel, F. O. (2019). Factors involved in relapse of multiple sclerosis. *Journal of Microscopy and Ultrastructure*, *7*(3), 103. https://doi.org/10.4103/JMAU.JMAU_59_18

Kantarci, O. H., & Weinshenker, B. G. (2005). Natural history of multiple sclerosis. In *Neurologic Clinics* (Vol. 23, Issue 1, pp. 17–38). https://doi.org/10.1016/j.ncl.2004.10.002

Kutzelnigg, A., & Lassmann, H. (2014). Pathology of multiple sclerosis and related inflammatory demyelinating diseases. *Handbook of Clinical Neurology*, *122*, 15–58. https://doi.org/10.1016/B978-0-444-52001-2.00002-9

Lassmann, H., Brück, W., & Lucchinetti, C. F. (2007). The immunopathology of multiple sclerosis: An overview. *Brain Pathology*, *17*(2), 210–218. https://doi.org/10.1111/j.1750-3639.2007.00064.x

Lebrun-Frenay, C., Kobelt, G., Berg, J., Capsa, D., & Gannedahl, M. (2017). New insights into the burden and costs of multiple sclerosis in Europe: Results for France. *Multiple Sclerosis Journal*, *23*(2_suppl), 65–77. https://doi.org/10.1177/1352458517708125

Lewis, D. A. (2002). The Human Brain Revisited: Opportunities and Challenges in Postmortem Studies of Psychiatric Disorders. *Neuropsychopharmacology 2002 26:2*, *26*(2), 143–154. https://doi.org/10.1016/s0893-133x(01)00393-1

Liney, G. (2006). *MRI in clinical practice* (Vol. 34, Issue 1).

Logan, J. (2000). Graphical analysis of PET data applied to reversible and irreversible tracers. *Nuclear Medicine and Biology*, *27*(7), 661–670. https://doi.org/10.1016/S0969-8051(00)00137-2

Love, S. (2006). Demyelinating diseases. *Journal of Clinical Pathology*, *59*(11), 1151–1159. https://doi.org/10.1136/jcp.2005.031195

Magliozzi, R., Howell, O. W., Reeves, C., Roncaroli, F., Nicholas, R., Serafini, B., Aloisi, F., & Reynolds, R. (2010). A Gradient of neuronal loss and meningeal inflammation in multiple sclerosis. *Annals of Neurology*, *68*(4), 477–493. https://doi.org/10.1002/ANA.22230

Morris, E. D., Endres, C. J., Schmidt, K. C., Christian, B. T., Muzic JR., R. F., & Fisher, R. E. (2004). Kinetic Modeling in Positron Emission Tomography. In *Emission Tomography*.

Ouchi, Y., Yoshikawa, E., Sekine, Y., Futatsubashi, M., Kanno, T., Ogusu, T., & Torizuka, T. (2005). Microglial activation and dopamine terminal loss in early Parkinson's disease. *Annals of Neurology*, *57*(2), 168–175. https://doi.org/10.1002/ana.20338

Owen, D. R., Yeo, A. J., Gunn, R. N., Song, K., Wadsworth, G., Lewis, A., Rhodes, C., Pulford, D. J., Bennacef, I., Parker, C. A., Stjean, P. L., Cardon, L. R., Mooser, V. E., Matthews, P. M., Rabiner, E. A., & Rubio, J. P. (2012). An 18-kDa Translocator Protein (TSPO) polymorphism explains differences in binding affinity of the PET radioligand PBR28. *Journal of Cerebral Blood Flow and Metabolism*, *32*(1). https://doi.org/10.1038/jcbfm.2011.147

Phelps, M. E., Huang, S. C., Hoffman, E. J., Selin, C., Sokoloff, L., & Kuhl, D. E. (1979). Tomographic measurement of local cerebral glucose metabolic rate in humans with (F-18)2-fluoro-2-deoxy-D-glucose: Validation of method. *Annals of Neurology*, *6*(5), 371–388. https://doi.org/10.1002/ANA.410060502

Rissanen, E. (2015). *Imaging Neuroinflammation In Progressive Multiple Sclerosis* (Doctoral dissertation, University of Turku). https://urn.fi/URN:ISBN:978-951-29-6099-6

Rizzo, G., Veronese, M., Tonietto, M., Zanotti-Fregonara, P., Turkheimer, F. E., & Bertoldo, A. (2014). Kinetic modeling without accounting for the vascular component impairs the quantification of [11C]PBR28 brain PET data. In *Journal of Cerebral Blood Flow and Metabolism* (Vol. 34, Issue 6, pp. 1060–1069). https://doi.org/10.1038/jcbfm.2014.55

Roussel, O. G., Ma, Y., & Evans, A. C. (1998). Correction for Partial Volume Effects in PET: Principle and Validation. *The Journal of Nuclear Medicine*, *39*(5), 904–911.

Russell, K. (2017). *Longitudinal in vivo monitoring of the neuropathology in ovine neuronal ceroid lipofuscinoses*. (Doctoral Dissertation, Lincoln University). https://hdl.handle.net/10182/9110

Sahab, Z. J., Semaan, S. M., & Amy Sang, Q.-X. (2007). Methodology and Applications of Disease Biomarker Identifi cation in Human Serum. *Biomarker Insights*, *2*, 21–43.

Salmon, T., Brooks, D. J., Leenders, K. L., Turton, D. R., Hume, S. P., Cremer, J. E., Jones, T., & Frackowiak, R. S. J. (1990). A Two-Compartment Description and Kinetic Procedure for Measuring Regional Cerebral [l1 C]Nomifensine Uptake U sing Positron Emission Tomography. *Journal of Cerebral Blood Flow and Metabolism*, *10*, 307–316.

Scalfari, A., Neuhaus, A., Daumer, M., Muraro, P. A., & Ebers, G. C. (2014). Onset of secondary progressive phase and long-term evolution of multiple sclerosis. *Journal of Neurology, Neurosurgery, and Psychiatry*, *85*, 67–75. https://doi.org/10.1136/jnnp-2012-304611

Sucksdorff, M., Matilainen, M., Tuisku, J., Polvinen, E., Vuorimaa, A., Rokka, J., Nylund, M., Rissanen, E., & Airas, L. (2020). Brain TSPO-PET predicts later disease progression independent of relapses in multiple sclerosis. *Brain*, *143*(11), 3318–3330. https://doi.org/10.1093/brain/awaa275

Tomasi, G., Edison, P., Bertoldo, A., Roncaroli, F., Singh, P., Gerhard, A., Cobelli, C., Brooks, D. J., & Turkheimer, F. E. (2008). Novel reference region model

reveals increased microglial and reduced vascular binding of11C-(R)-PK11195 in patients with Alzheimer's disease. *Journal of Nuclear Medicine*, *49*(8), 1249–1256. https://doi.org/10.2967/jnumed.108.050583

Tuisku, J. (2021). *Imaging Of Neuroinflammation In Multiple Sclerosis Brain:a positron emission tomography and diffusion tensor imaging study*. (Doctoral Dissertation, University of Turku). https://urn.fi/URN:ISBN:978-951-29-8485-5

Tuisku, J., Plavén-Sigray, P., Gaiser, E. C. , Airas, L., Al-Abdulrasul, H., Brück, A., Carson, R. E., Chen, M.-K., Cosgrove, K. P., Ekblad, L., Esterlis, I., Farde, L., Forsberg, A., Halldin, C., Helin, S., Kosek, E., Lekander, M., Lindgren, N., Marjamäki, P., … Cervenka, S. (2019). Effects of age, BMI and sex on the glial cell marker TSPO — a multicentre [11C]PBR28 HRRT PET study. *European Journal of Nuclear Medicine and Molecular Imaging*, *46*(11), 2329–2338. https://doi.org/10.1007/s00259-019-04403-7

Turkheimer, F. E., Edison, P., Pavese, N., Roncaroli, F., Anderson, A. N., Hammers, A., Gerhard, A., Hinz, R., Tai, Y. F., & Brooks, D. J. (2007). Reference and target region modeling of [11C]-(R)-PK11195 brain studies. *Journal of Nuclear Medicine*, *48*(1).

Turkheimer, F. E., Rizzo, G., Bloomfield, P. S., Howes, O., Zanotti-Fregonara, P., Bertoldo, A., & Veronese, M. (2015). The methodology of TSPO imaging with positron emission tomography. *Biochemical Society Transactions*, *43*, 586–592. https://doi.org/10.1042/BST20150058

Turkheimer, F. E., Veronese, M., & Dunn, J. (2014). *Experimental Design and Practical Data Analysis in Positron Emission Tomography* (1st ed.). Published independently with CreateSpace.

Tzourio-Mazoyer, N., Landeau, B., Papathanassiou, D., Crivello, F., Etard, O., Delcroix, N., Mazoyer, B., & Joliot, M. (2002). Automated Anatomical Labeling of Activations in SPM Using a Macroscopic Anatomical Parcellation of the MNI MRI Single-Subject Brain. *NeuroImage*, *15*(1), 273–289. https://doi.org/10.1006/NIMG.2001.0978

van den Hoff, J., Lougovski, A., Schramm, G., Maus, J., Oehme, L., Petr, J., Beuthien-Baumann, B., Kotzerke, J., & Hofheinz, F. (2014). Correction of scan time dependence of standard uptake values in oncological PET. In *EJNMMI Research, 4, 1-18.* http://www.ejnmmires.com/content/4/1/18http://www.ejnmmires.com/content/4/1/18

Venneti, S., Lopresti, B. J., & Wiley, C. A. (2006). The peripheral benzodiazepine receptor (Translocator protein 18 kDa) in microglia: From pathology to imaging. *Progress in Neurobiology*, *80*(6), 308–322. https://doi.org/10.1016/j.pneurobio.2006.10.002

Veronese, M., Reis Marques, T., Bloomfield, P. S., Rizzo, G., Singh, N., Jones, D., Agushi, E., Mosses, D., Bertoldo, A., Howes, O., Roncaroli, F., & Turkheimer, F. E. (2018). Kinetic modelling of [11 C]PBR28 for 18 kDa translocator protein PET data: A validation study of vascular modelling in the brain using XBD173 and tissue analysis. *Journal of Cerebral Blood Flow and Metabolism*, *38*(7), 1227–1242. https://doi.org/10.1177/0271678X17712388

Wallin, M. T., Culpepper, W. J., Nichols, E., Bhutta, Z. A., Gebrehiwot, T. T., Hay, S. I., Khalil, I. A., Krohn, K. J., Liang, X., Naghavi, M., Mokdad, A. H., Nixon, M. R., Reiner, R. C., Sartorius, B., Smith, M., Topor-Madry, R., Werdecker, A., Vos, T., Feigin, V. L., & Murray, C. J. L. (2019). Global, regional, and national burden of multiple sclerosis 1990–2016: a systematic analysis for the Global Burden of Disease Study 2016. *The Lancet Neurology*, *18*(3), 269–285. https://doi.org/10.1016/S1474-4422(18)30443-5

Weinshenker, B. G. (1995). The Natural History of Multiple Sclerosis [Article]. *Neurologic Clinics*, *13*(1), 119–146. https://doi.org/10.1016/S0733-8619(18)30064-1

Yaqub, M., van Berckel, B. N. M., Schuitemaker, A., Hinz, R., Turkheimer, F. E., Tomasi, G., Lammertsma, A. A., & Boellaard, R. (2012a). Optimization of supervised cluster analysis for extracting reference tissue input curves in (R)-[11C]PK11195 brain PET studies. *Journal of Cerebral Blood Flow and Metabolism*, *32*(8), 1600–1608. https://doi.org/10.1038/jcbfm.2012.59

Ziemssen, T., Akgün, K., & Brück, W. (2019). Molecular biomarkers in multiple sclerosis. *Journal of Neuroinflammation*, *16*(1). https://doi.org/10.1186/s12974-019-1674-2